doi: 10.2166/9781780409566

Chapter 10

Nutrient recovery from water and wastewater

Robert Colston[1], Stephan Tait[2], Céline Vaneeckhaute[3], Heidy Cruz[4], Ilje Pikaar[5], Thomas Seviour[6], Johannes B. M. Klok[7,8], Jan Weijma[9], Henk Dijkman[10], Cees J. N. Buisman[7,9], Sasha Scattergood[11], Ana A. Robles-Aguilar[12], Erik Meers[1], Fabrice Béline[13] and Ana Soares[1]

[1]*Cranfield Water Science Institute, Vincent Building, Cranfield University, Cranfield, Beds, MK43 0AL, UK*
[2]*Centre for Agricultural Engineering, University of Southern Queensland, Toowoomba, Queensland, 4350, Australia*
[3]*Research team on green process engineering and biorefineries (BioEngine), Chemical Engineering Department, Université Laval, 1065 avenue de la Médecine, Québec, QC, Canada*
[4]*Civil and Environmental Engineering Department, National University of Singapore, 1 Engineering Drive 2, #07-03 E1A, 117576, Singapore*
[5]*The School of Civil Engineering, The University of Queensland, St Lucia, QLD 4072, Australia*
[6]*WATEC Aarhus University Centre for Water Technology, Nørrebrogade 44, Bldg 1783, 8000 Aarhus, Denmark*
[7]*Wetsus, the Netherlands*
[8]*Paqell B.V., the Netherlands*
[9]*Wageningen University & Research, the Netherlands*
[10]*Paques B.V., the Netherlands*
[11]*Anaergia Inc., Burlington, ON, Canada*
[12]*Faculty of Bioscience Engineering, Ghent University, Belgium*
[13]*Irstea – National Institute for Environmental and Agricultural Science and Research, Rennes, France*

10.1 INTRODUCTION

Nitrogen (N), phosphorus (P) and sulfur (S) are essential nutrients and key to food production security, and primary components of fertilizers, for example for agriculture, energy crops (e.g., bioethanol) and aquaculture. They are also used in the pharmaceutical, chemical, automotive and aerospace industries to produce chemicals, medicines, smart devices, aeroplanes parts and car batteries and so on. Hence, nutrients are critical to a number of industries. N, P and S production is costly and resource intensive. For example, the Haber–Bosch process for N fertilizer production represents about 1–2% of the total world energy consumption (Matassa *et al.*, 2015). It uses non-renewable natural gas, and is responsible for an estimated 1.2% of greenhouse emissions worldwide. Moreover, P is a 'disappearing nutrient' and was placed on the Critical Raw Material (CRM) list in 2014 by the European Commission. This is a critical problem in the agricultural sector since P, together with N and potassium, are the main macronutrients for inorganic fertilizers. S is similarly an important agricultural nutrient, atmospheric S deposits continue to decline, and intensification of agriculture has taken up high amounts of S in soils (Hinckley *et al.*, 2020).

Wastewater is a rich source of N, P and S. N enters as ammonium and organic N from urine and industrial discharges, P from phosphates from human and animal wastes, detergents, and food wastes, and S as sulfate or sulfide from chemical coagulants in drinking water production, human wastes, and industrial discharges (Egle *et al.*, 2015; Galloway *et al.*, 2014; Pikaar *et al.*, 2014). The traditional focus of wastewater treatment processes has been to remove nutrients in order to protect public health, assets, and the environment. This is because excessive N and P in water leads to eutrophication which damages aquatic ecosystems (Robles *et al.*, 2020). Moreover, high S loadings in wastewater treatment plants (WWTPs) lead to noxious gaseous emissions, corrosion (e.g., pipes), inhibition of wastewater microbial activities, and acid rain if biosolids or biogas are combusted. Sulfide-induced concrete corrosion has been recognized as the main cause of sewer system deterioration (Pikaar *et al.*, 2014).

WWTPs have typically employed biological approaches to remove N via destructive dissipative processes and a combination of chemical and biological treatments to remove P from municipal wastewaters (McCarty, 2018; Oehmen *et al.*, 2007). S removal from municipal wastewaters is not currently widely implemented. Given the increasing demand in fertilizers to meet global food demands, however, the importance and urgency of recovering nutrients continues to grow. Consequently there has been much interest in technologies that can recover N, P and S from wastewater.

Technologies used to recover N, P and S from wastewater will be discussed in this chapter and include:

- P recovery, specifically by formation of the mineral struvite, from centrate or P-rich agricultural/industrial wastewaters; and
- N recovery via ammonia removal by stripping and subsequent recovery, as applied to high strength industrial waters (e.g., landfill leachates) and digestate from anaerobic digestion;
- Elemental S recovery by bio-conversion to H_2S, and subsequent absorption and/or oxidation. The same process can be applied to treat industrial off-gases rich in H_2S.

The principles, technologies and case studies for these nutrient recovery processes are presented here, along with relevant challenges and opportunities for N, S and P recovery.

10.2 LEARNING OBJECTIVES

At the completion of this chapter you should be able to:

- Explain the fundamental principles of struvite formation, ammonia stripping/absorption, and sulfur conversion and recovery processes.
- Describe the key design criteria and performance parameters for relevant nutrient recovery processes.
- Characterize and examine specific challenges for struvite precipitation, ammonia stripping and sulfur recovery processes, given specific case studies.
- Evaluate resource recovery options for struvite precipitation, ammonia stripping/absorption and sulfur recovery processes, given a specific application scenario and water composition.

10.3 PHOSPHORUS RECOVERY – THE ESSENTIAL AND DWINDLING NUTRIENT

P is an essential nutrient, and has no substitute in biological functions. Shortages threaten global food security, which are exacerbated by rising population. Moreover, the movement from fossil fuels to biofuels increases P demand, as the growing market for fuel crops further increases the demand for fertilizers (Reijnders, 2014). Technological development has also found use for P in pharmaceuticals, household and energy products, placing further pressure on P supply (Chen *et al.*, 2019; Reijnders, 2014; Yan *et al.*, 2018). It is estimated that the current use of P globally is >30 million tons year^{-1} (Reijnders, 2014).

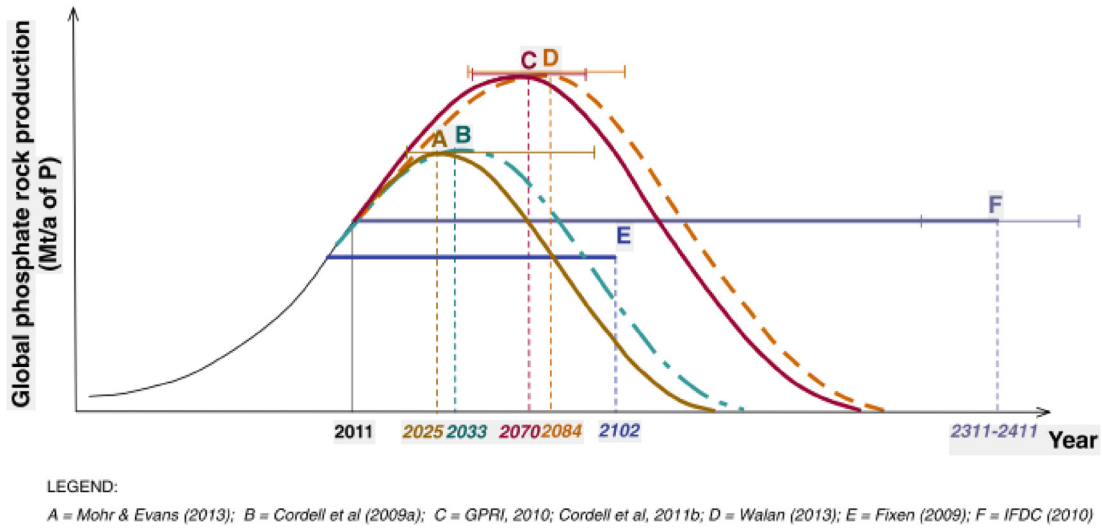

Figure 10.1 Various rock phosphate peak production estimates and depletion rates (with permission from Cordell and White (2015)).

Increased use of fertilizers has led to widespread environmental problems, such as enhanced eutrophication effects which has caused widespread algal blooms. This is detrimental to ecosystems as algal blooms reduce the concentration of nutrients available and the penetration of sunlight into the photic zone. The reduced primary productivity and anoxia that ensue threaten the local food chain. Furthermore, algal blooms can be toxic (Sekula-Wood *et al.*, 2009), and impact on utilities and services, such as bathing water quality control and tourism.

Non-renewable P is predominately refined from the apatite group ($Ca_5(PO_4)_3(OH, F, Cl)$). Apatite deposits are heterogeneous occurring in many geological settings. This poses problems when estimating global P reserves. Current estimates for when P reserves will be depleted and thus vary widely from 100 to 400 years (Figure 10.1). Estimates in phosphate ore reserves range from 70 to 300 billion tons (U.S. Geological Survey, 2019) and research models estimate that there are between 67 and 110 billion tons of refined phosphate (25–30 wt% P_2O_5) (Springer, 2017). The uncertainty about availability contributes to a very volatile ore-born P market and pricing.

A recent census showed EU members import nearly 100% of their phosphate fertilizers (Figure 10.2). To cope with increasing fertilizer demand, the EU have put in place several protocols to reduce the use of P where possible, such as reducing the concentrations of P in washing detergents (De Ridder *et al.*, 2012), thereby relieving pressures on P demand and reducing P input from grey wastewater. Regardless, alternative strategies for reducing dependence on P imports and recycling nutrients are required to ensure food security.

10.3.1 Conceptual overview – struvite precipitation

Active P recovery from wastewater has been implemented for the past 20 years or so in various different forms. The most common P-rich material recovered is struvite. It has been estimated that in 2020 between 990 and 1250 ton P was recovered as struvite in the EU (Muys *et al.*, 2021).

Struvite precipitation occurs by a phase change where the constituent ions, magnesium (Mg^{2+}), ammonium (NH_4^+) and phosphate (PO_4^{3-}), previously dissolved in wastewater, precipitate out to form

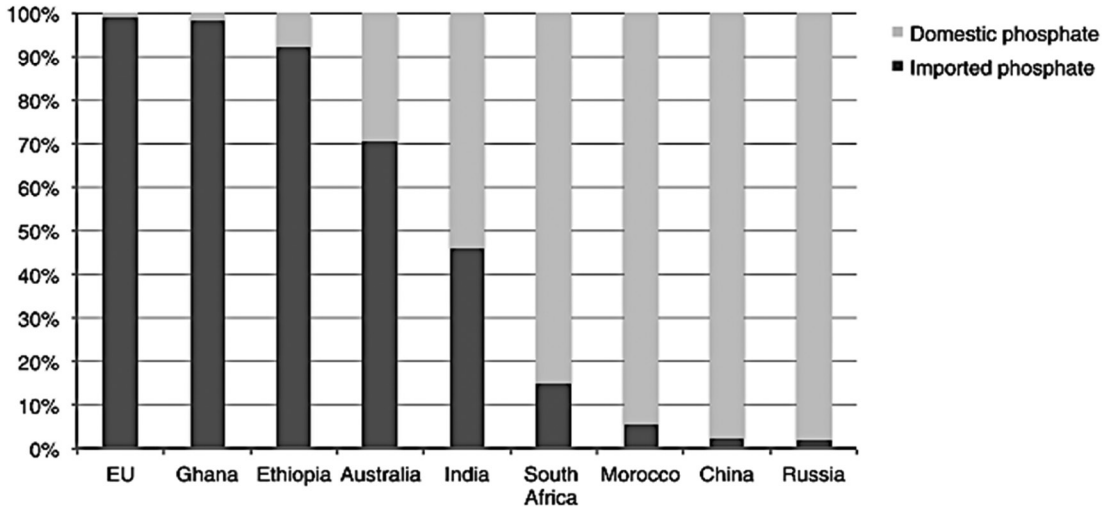

Figure 10.2 Nations' dependence on imported phosphate fertilizers as of 2010 (with permission from Cordell and White (2015)).

a crystalline mineral called struvite ($NH_4MgPO_4 \cdot 6H_2O(s)$). The struvite precipitation reaction is as follows:

$$Mg^{2+}(aq) + NH_4^{+}(aq) + PO_4^{3-}(aq) + 6H_2O \leftrightarrow NH_4MgPO_4 \cdot 6H_2O(s) \quad (10.1)$$

Six water molecules are bound in the crystal structure per mole of struvite formed. The struvite crystals can then be separated from the wastewater, enabling the recovery of N as ammonia and P as phosphate. The usefulness of the struvite process lies in:

- struvite formation upconcentrating N and P from the wastewater liquid phase by as much as 2–3 orders of magnitude into the mineral solid phase; and
- the struvite crystal being highly selective for Mg^{2+}, NH_4^{+} and PO_4^{3-}, resulting in a high struvite purity and excluding contaminants in the bulk wastewater phase.

To form struvite, N and P have to be in mineralized form (i.e., P as phosphate and N as ammonium). Within the water/wastewater context, organic P and organic N are biologically hydrolyzed into phosphate and ammoniacal N, respectively. This often causes maintenance challenges around WWTPs, when conditions become conducive to struvite forming in unwanted places in pipes, pumps and equipment, causing inorganic scale issues requiring frequent maintenance (Figure 10.3) (Le Corre, 2006; Shaddel *et al.*, 2019). However, the intentional minerals precipitation process, as outlined in this chapter, aims to promote struvite formation in a controlled way in a reaction vessel. This has the added benefit of preventing its unwanted formation in other parts of a WWTP.

10.3.1.1 Factors affecting struvite precipitation – equilibrium and solubility

Struvite precipitation is bi-directional reaction (indicated by a bi-directional arrow in Equation (10.2)). This means that the reaction occurs significantly and simultaneously in both the forwards and the backwards directions, resulting in simultaneous formation and dissolution of struvite, respectively. Bi-directional reactions eventually attain equilibrium and then satisfy an equilibrium relationship.

Figure 10.3 Unwanted inorganic scale within water pipework.

The equilibrium relationship for struvite is typically written for the reaction with the mineral phase on the left hand side as follows (the reverse of Equation (10.1) above):

$$NH_4MgPO_4 \bullet 6H_2O(s) \rightleftarrows Mg^{2+}(aq) + NH_4{}^{+}(aq) + PO_4{}^{3-}(aq) + 6H_2O \tag{10.2}$$

with the corresponding equilibrium relationship being:

$$K_{sp,struv} = \left(Mg^{2+}(aq)\right)_{eq} \times \left(NH_4{}^{+}(aq)\right)_{eq} \times \left(PO_4{}^{3-}(aq)\right)_{eq} \tag{10.3}$$

where $K_{sp,struv}$ is the equilibrium constant ($10^{-13.26}$ (Ohlinger *et al.*, 1998)), dependent only on temperature (and to a lesser extent pressure), and $(Mg^{2+}(aq))_{eq}$, $(NH_4{}^{+}(aq))_{eq}$, $(PO_4{}^{3-}(aq))_{eq}$ are chemical activities of the participating ions representing their 'reactive concentrations'. Note that the equilibrium relationship does not include the chemical activities of struvite and water, because these are equal to 1 with wastewater being mostly water and struvite being considered a mostly pure crystalline substance.

The equilibrium relationship formulated in terms of concentrations of ions in solution applies a multiplier-correction as follows:

$$(X) = [X] \times \gamma_i \tag{10.4}$$

where $[X]$ is the concentration of the hypothetical compound X, γ_i is its multiplier correction factor commonly termed an activity coefficient, and (X) is the chemical activity as above. The equilibrium relationship for struvite is then expanded as follows:

$$\begin{aligned} K_{sp,struv} = &\left(\gamma_{Mg} \times \left[Mg^{2+}(aq)\right]_{eq}\right) \times \left(\gamma_{NH_4} \times \left[NH_4{}^{+}(aq)\right]_{eq}\right) \\ &\times \left(\gamma_{PO_4} \times \left[PO_4{}^{3-}(aq)\right]_{eq}\right) \end{aligned} \tag{10.5}$$

where $[Mg^{2+}(aq)]_{eq}$, $[NH_4{}^{+}(aq)]_{eq}$, $[PO_4{}^{3-}(aq)]_{eq}$ are the concentrations of the respective ions in the wastewater at equilibrium and γ_{Mg}, γ_{NH4} and γ_{PO4} are their respective activity coefficients.

The value of the activity coefficient is commonly estimated by an empirical correlation. One such correlation which is commonly used is the Davies equation, which is affected by the charge or valency (z_x) of a respective constituent (X) as follows:

$$\log_{10}(\gamma_i) = -\mathrm{A}z_x^2(I^{1/2}/(1+I^{1/2}) - 0.24I) \tag{10.6}$$

where A is a constant ($= 0.5085\ \mathrm{M}^{-1/2}$ at 25°C) that depends on the dielectric constant and temperature, and I is the ionic strength of the wastewater liquid solution, calculated as follows:

$$I = 1/2\Sigma_i m_i z_i^2 \tag{10.7}$$

where m_x is the molal concentration (mol/kg) of the respective constituent, which for a typical wastewater can be approximated as its molar concentration (mol/L). The Davies equation appears to be comparable to other more complex activity coefficient models up to $I = 0.2$ molal (Tait *et al.*, 2012). Activity coefficients of neutral ion pairs (see further below) can also be estimated as follows:

$$\log_{10}(\gamma_i) = \alpha_1 I \tag{10.8}$$

where α_1 is 0.1. Following the form of the equilibrium relationship in Equation (10.6), it is common to calculate an ion activity product (IAP) as follows:

$$\begin{aligned}\mathrm{IAP}_{\mathrm{struv}} = &\left(\gamma_{\mathrm{Mg}} \times \left[\mathrm{Mg}^{2+}(\mathrm{aq})\right]\right) \times \left(\gamma_{\mathrm{NH_4}} \times \left[\mathrm{NH_4}^{+}(\mathrm{aq})\right]\right) \\ &\times \left(\gamma_{\mathrm{PO_4}} \times \left[\mathrm{PO_4}^{3-}(\mathrm{aq})\right]\right)\end{aligned} \tag{10.9}$$

where in this case the concentrations of the respective ions may not be at equilibrium.

A mathematical variant of Equation (10.9), commonly termed the saturation index (SI) value, is calculated as follows:

$$\mathrm{SI}_{\mathrm{struv}} = \log_{10}\left(\frac{\mathrm{IAP}_{\mathrm{struv}}}{K_{\mathrm{sp,struv}}}\right) \tag{10.10}$$

$\mathrm{SI}_{\mathrm{struv}}$ and $\mathrm{IAP}_{\mathrm{struv}}$ are very important for design and operation of struvite precipitation processes and are also used to predict and prevent inorganic scale formation. If $\mathrm{IAP}_{\mathrm{struv}} > K_{\mathrm{sp,struv}}$ (i.e., $\mathrm{SI}_{\mathrm{struv}} > 0$), then struvite will precipitate to attain equilibrium (Equation (10.3)). Such conditions are commonly referred to as 'supersaturated'. In contrast, if $\mathrm{IAP}_{\mathrm{struv}} < K_{\mathrm{sp,struv}}$ (i.e., $\mathrm{SI}_{\mathrm{struv}} < 0$) and if struvite mineral phase is present, then the struvite will want to dissolve to attain equilibrium (Equation (10.1)). Such conditions are commonly referred to as 'unsaturated'.

When $\mathrm{IAP}_{\mathrm{struv}} = K_{\mathrm{SP,struv}}$, then $\mathrm{SI}_{\mathrm{struv}} = 0$ and conditions are at equilibrium, representing the solubility conditions of struvite in the wastewater.

Equation (10.9) importantly shows that struvite precipitation can be induced by adding any of the participating ions as a chemical reagent. For example, to induce struvite formation to remove and recover $\mathrm{PO_4}^{3-}$ and $\mathrm{NH_4}^{+}$, Mg^{2+} can be added as magnesium chloride, magnesium oxide, magnesium hydroxide or other, to increase $\mathrm{IAP}_{\mathrm{struv}}$ so that $\mathrm{SI}_{\mathrm{struv}} > 0$. This is common practice with struvite reactors.

10.3.1.2 Factors affecting struvite precipitation – Ion pairing

The struvite precipitation reaction competes with ion pairing reactions for ions in the wastewater liquid phase. These reactions occur in the wastewater liquid phase and form ion pairs without undergoing a phase change. Some relevant ion pairs that compete with struvite include the reactions:

$$\mathrm{Mg}^{2+}(\mathrm{aq}) + \mathrm{PO_4}^{3-}(\mathrm{aq}) \leftrightarrow \mathrm{MgPO_4}^{-}(\mathrm{aq}) \tag{10.11}$$

and

$$H^{+}(aq) + PO_4^{-3}(aq) \leftrightarrow HPO_4^{2-}(aq) \tag{10.12}$$

which compete with struvite precipitation for $Mg^{2+}(aq)$ (Equation (10.11)) and $PO_4^{-3}(aq)$ (Equations (10.11) and (10.12)). This must be considered in the design and operation of struvite precipitation processes. Some ion pairs carry a charge ($MgPO_4^{-}(aq)$), while others are uncharged ($MgHPO_4(aq)$), and this influences the activity coefficient calculations (Equations (10.6) and (10.8)). Some ion pairing reactions are weak acid-base reactions (Equation (10.12)) and this influences struvite precipitation via pH of a wastewater, by increasing or decreasing the competition with a weak acid-base ion pair. This is illustrated in Figure 10.4 which shows a phase diagram for struvite in a wastewater with phosphate as the limiting reagent. Generally, higher pH tends to favor the formation of struvite because it reduces competition with the weak acid-base phosphate system, specifically for $PO_4^{-3}(aq)$ (Figure 10.4). However, high pH conditions can inadvertently exist in filters and turbulent flow areas, when localized aeration causes CO_2 stripping and a pH increase, amd this is a cause for unwanted struvite scale formation in such locations (Le Corre, 2006).

Fortunately, ion pairing reactions are rapid when compared to the struvite precipitation reaction. Consequently, ion pairing reactions are usually at equilibrium and their impact on struvite precipitation can be readily estimated using well-established aqueous equilibrium models. Such models are available as standalone software packages (e.g., PhreeqC, introduced in this chapter) or have been incorporated into commercial wastewater modelling packages (e.g., BioWin, Sumo19). These models calculate the resulting free ion concentrations $[Mg^{2+}(aq)]_{eq}$, $[NH_4^{+}(aq)]_{eq}$ and $[PO_4^{3-}(aq)]_{eq}$ at equilibrium with the various relevant ion pairs, and then these concentrations can be used to calculate IAP_{struv} or SI_{struv} via Equations (10.9) and (10.10). These can then be used to determine if a wastewater is supersaturated or undersaturated, and thus whether struvite will precipitate or dissolve.

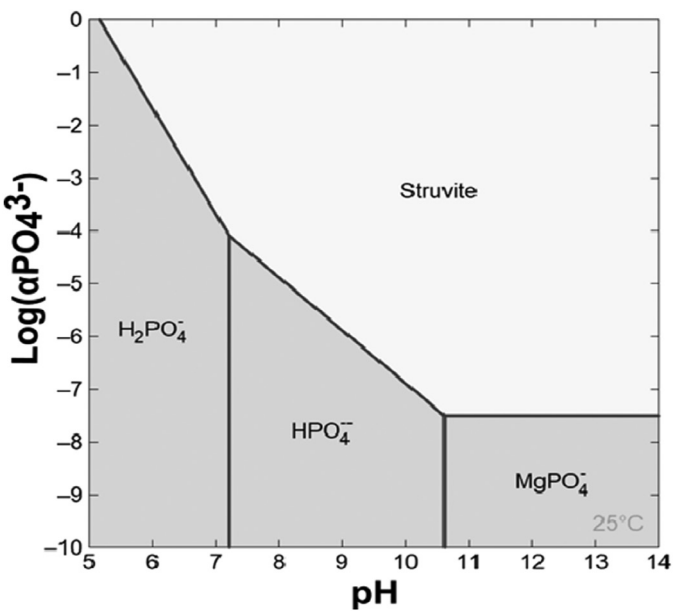

Figure 10.4 Phase diagram for ion pairing and struvite in water, with phosphate as limiting reagent. The diagram illustrates the effect of the phosphate weak acid-base system via pH and the influence of an ion pair with magnesium.

10.3.1.3 Worked exercise 1a

As an illustrated example consider a wastewater containing 200 mg P/L as phosphate, 1000 mg N/L as ammoniacal N (i.e., $NH_4^+(aq) + NH_3(aq)$), 100 mg Mg/L and 2550 mg/L of choride as measured by an analytical laboratory (these are total concentrations and include all ion pairs and free ions), at pH 6.12 and 25°C. We will use the model software package PhreeqC with the Minteq.dat model database to determine whether this wastewater is supersaturated or undersaturated with respect to struvite.

PhreeqC is available for download at https://www.usgs.gov/software/phreeqc-version-3. PhreeqC is free to use within the constraints of its User Rights Notice, available at https://water.usgs.gov/water-resources/software/PHREEQC/Phreeqc_UserRightsNotice.txt. The wastewater composition above is entered into PhreeqC, and the thermodynamic database used by the model is set to Minteq.dat. Figure 10.5 presents a screenshot of the text-based coding window corresponding to the wastewater composition input.

When the model is run, the following concentrations are calculated:

$[\text{Total } PO_4^*] = 200 \text{ mg P/L} = 6.482 \times 10^{-3} \text{ molal};$
$[\text{Total Mg}^*] = 100 \text{ mg Mg/L} = 4.129 \times 10^{-3} \text{ molal};$
$[\text{Total } NH_4^*] = 1000 \text{ mg N/L} = 7.167 \times 10^{-2} \text{ molal};$

*again, these are total concentrations, including the free-form ion and all ion pairs.

Ion pair and free form ion concentrations are determined by the model, as shown in Figure 10.6.

Figure 10.6 shows that a large proportion of the phosphate and a moderate proportion of the magnesium in the wastewater is paired with other ions as follows:

$$[PO_4^{-3}(aq)]/[\text{Total } PO_4^*] = 1.54 \times 10^{-9}/6.482 \times 10^{-3} = 2.376 \times 10^{-7}$$

with $H_2PO_4^-(aq)$ representing the majority ion pair with phosphate, and

$$[Mg^{2+}(aq)]/[\text{Total Mg}^*] = 3.49 \times 10^{-3}/4.129 \times 10^{-3} = 0.845$$

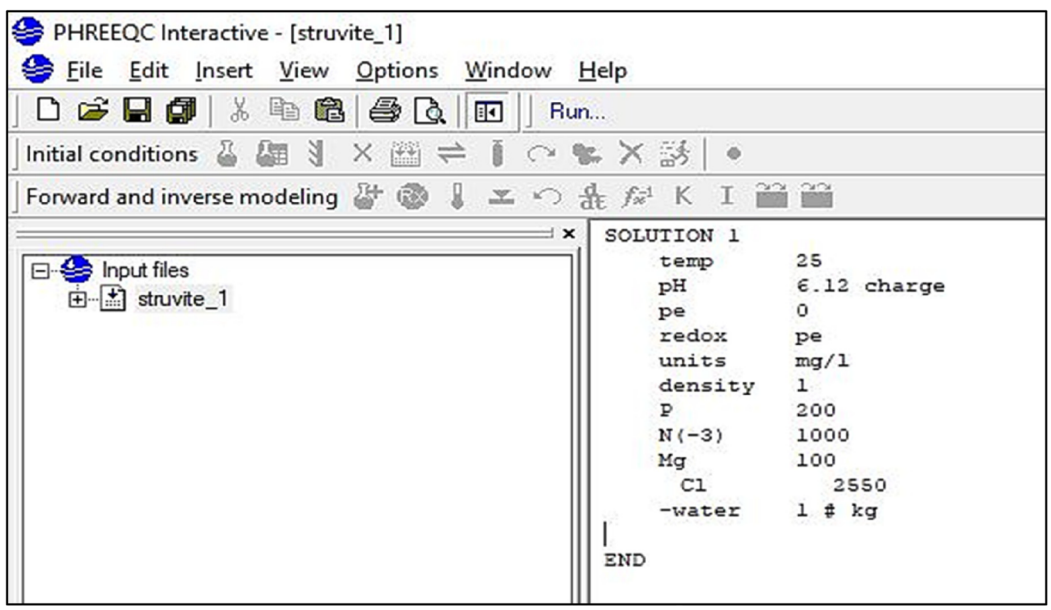

Figure 10.5 Simulation coding window (input) for PhreeqC simulation – Step 1a.

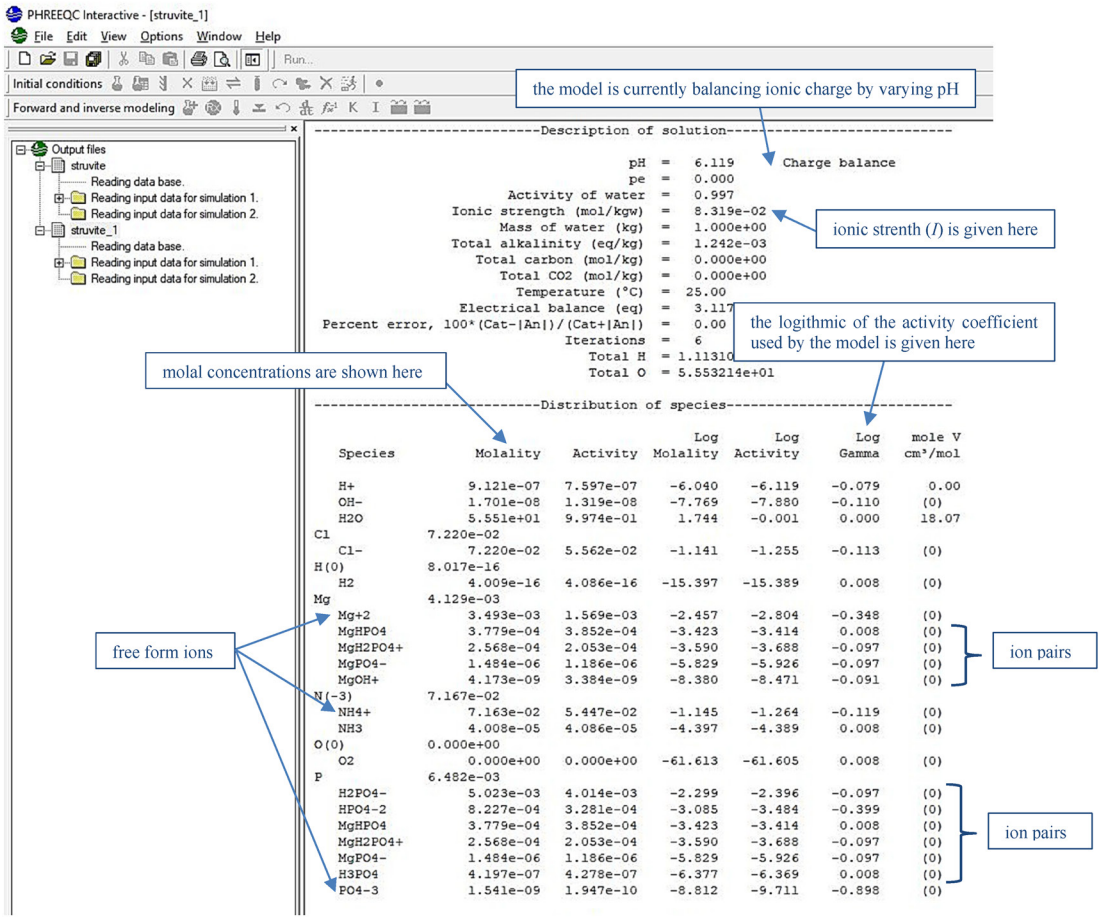

Figure 10.6 Simulation results window (output) for PhreeqC simulation – Step 1a.

with $MgHPO_4$ representing the majority ion pair with magnesium, and as a result the concentrations of the free ions that participate in struvite formation are $[PO_4^{-3}(aq)] = 1.54 \times 10^{-9}$ molal; $[Mg^{+2}(aq)] = 3.49 \times 10^{-3}$ molal; and $[NH_4^{+}(aq)] = 7.16 \times 10^{-2}$ molal. PhreeqC also calculates activity coefficients (e.g., Davies equation, Equation (10.6)) and estimates the ionic strength ($I = 0.08319$ molal) for this purpose.

Figure 10.6 shows the following activity coefficients: $\log_{10}(\gamma_{Mg2+}) = -0.348$ so $\gamma_{Mg2+} = 0.449$; $\log_{10}(\gamma_{NH4+}) = -0.119$ so $\gamma_{NH4+} = 0.760$; $\log_{10}(\gamma_{PO4\text{-}3}) = -0.898$ so $\gamma_{PO4\text{-}3} = 0.126$.

IAP_{struv} and SI_{struv} at these wastewater conditions can then be calculated as follows:

$$\begin{aligned} IAP_{struv} &= \left(\gamma_{Mg} \times \left[Mg^{2+}(aq)\right]\right) \times \left(\gamma_{NH_4} \times \left[NH_4^{+}(aq)\right]\right) \times \left(\gamma_{PO_4} \times \left[PO_4^{3-}(aq)\right]\right) \\ &= (0.449 \times 3.49 \times 10^{-3} \times 0.760 \times 7.16 \times 10^{-2} \times 0.126 \times 1.54 \times 10^{-9}) \\ &= 1.655 \times 10^{-14} \text{ or } 10^{-13.78} \quad (K_{sp,struv} = 10^{-13.26}) \end{aligned}$$

and

$$SI_{struv} = \log_{10}\left(\frac{IAP_{struv}}{K_{sp,struv}}\right) = \log_{10}\left(\frac{10^{-13.78}}{10^{-13.26}}\right) = -0.521$$

which shows that $IAP_{struv} < K_{sp,struv}$ and $SI_{struv} < 0$ and that the wastewater conditions are undersaturated with respect to struvite. Hence, struvite will not form, and if the mineral phase was present it will instead dissolve to attain equilibrium.

10.3.1.4 Worked exercise 1b

If sodium hydroxide (NaOH) was added to the wastewater in exercise 1a above, so that the amount of sodium in the wastewater composition is now instead 184 mg/L, the PhreeqC model can calculate the resulting increase in pH using an ionic charge balance. The modelling input and outputs are shown in Figures 10.7 and 10.8, respectively. Note how the equilibrium data for struvite precipitation has now been added into the model (Figure 10.7) because it was not previously in the model database. In the coding, log_k refers to the common logarithm of the solubility product constant, which in the case of struvite is –13.26 ($K_{sp,struv} = 10^{-13.26}$).

The results show that pH of the wastewater will rise to 7.98. Moreover, the simulation now gives free ions concentrations of $[PO_4^{-3}(aq)] = 6.098 \times 10^{-7}$ molal; $[Mg^{+2}(aq)] = 2.402 \times 10^{-3}$ molal; $[NH_4^{+}(aq)] = 6.890 \times 10^{-2}$ molal; and $I = 0.08849$ molal, from which $IAP_{struv} = 10^{-11.40} > K_{sp,struv}$ and $SI_{struv} = 1.86$. These show that by adding NaOH to increase the wastewater pH, conditions have been

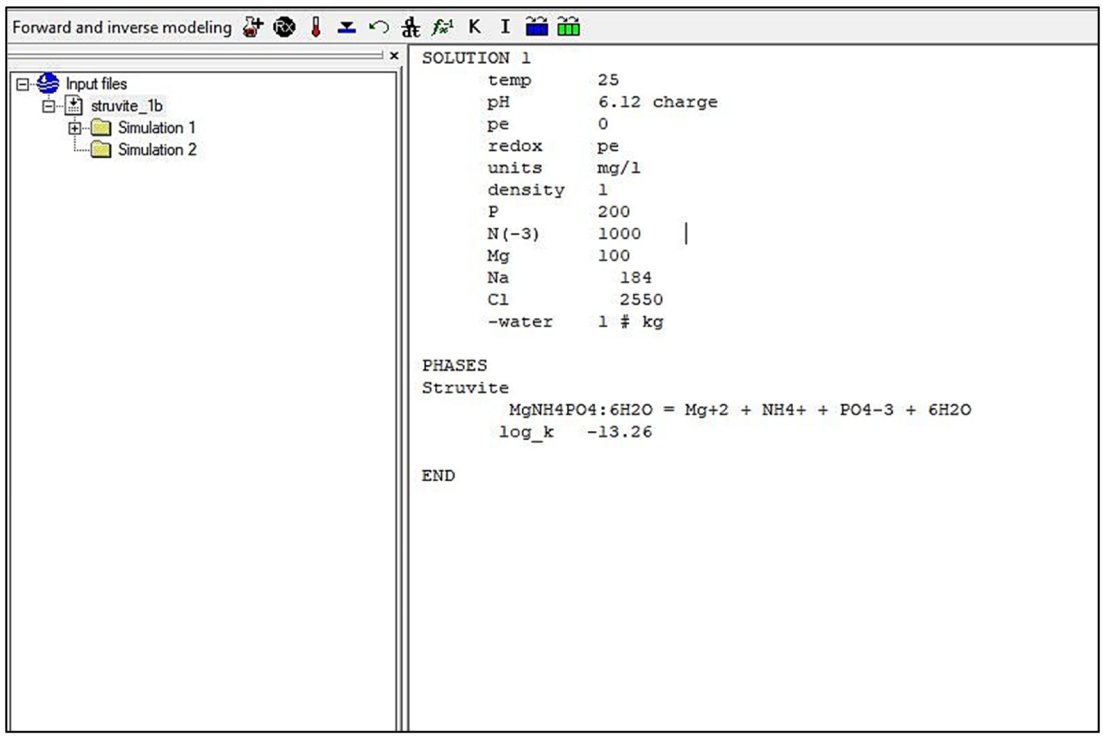

Figure 10.7 Simulation coding window (input) for PhreeqC simulation – Step 1b.

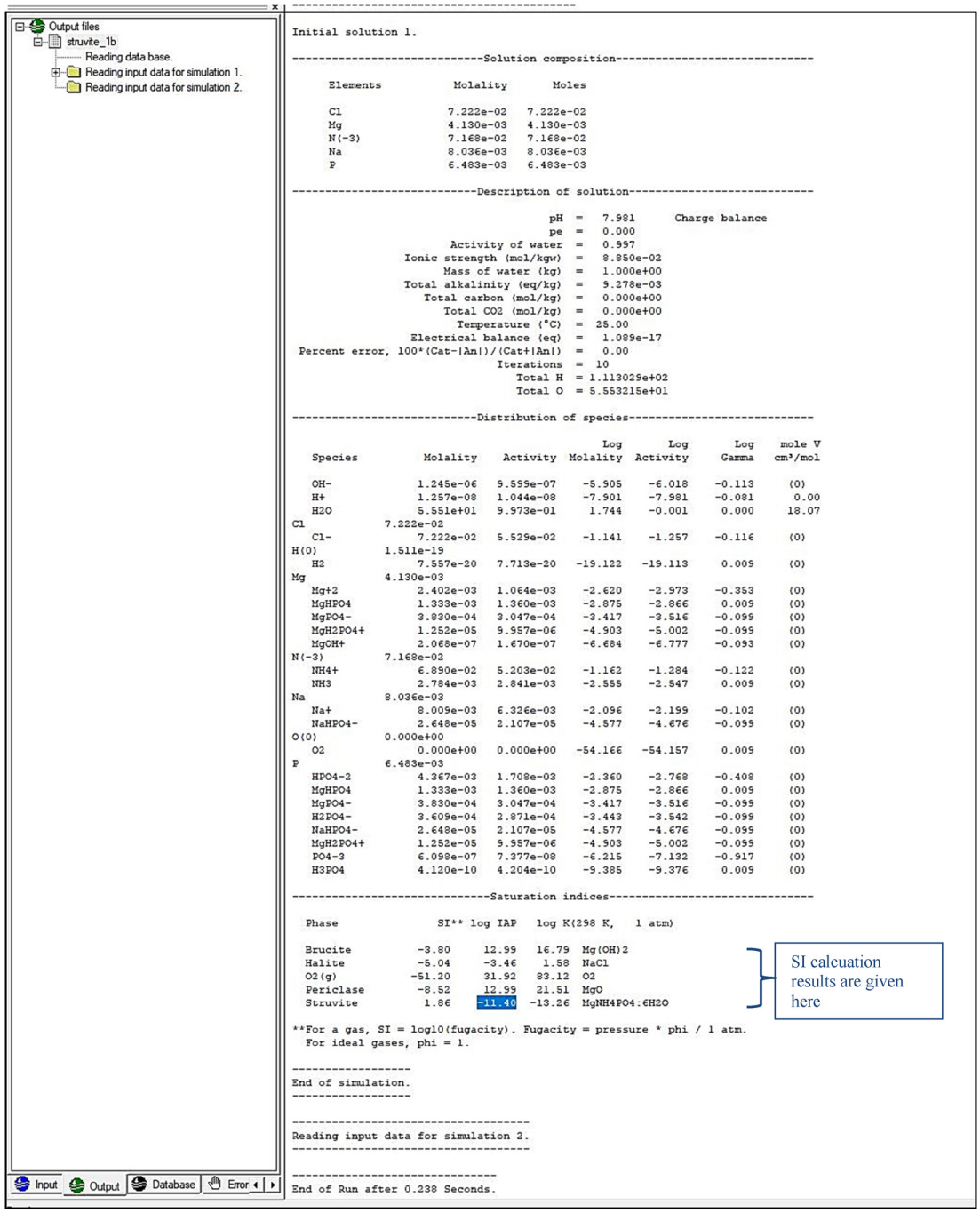

Figure 10.8 Simulation results window (output) for PhreeqC simulation – Step 1b.

changed from being undersaturated to being supersaturated, and instead struvite can now precipitate to attain equilibrium. This is primarily because the proportion of [PO_4^{-3}(aq)]/[Total PO_4*] has increased by decreasing the level of competition with the phosphate weak acid-base system.

10.3.1.5 Struvite nucleation, crystal growth and crystal morphology

Struvite precipitation occurs by new crystals nucleating and then growing and/or existing struvite crystals growing (Figure 10.9). Nucleation generally requires higher levels of supersaturation than for growth because, for nucleation to occur, a chemical energy barrier has to be overcome to produce nuclei (Mersmann, 2001). There are two main types of nucleation, primary nucleation which occurs in the absence of any pre-existing crystals, or secondary nucleation which occurs in the presence of at least one crystal (Mersmann, 2001).

The level of supersaturation required for primary nucleation to occur is usually greater than for secondary nucleation to occur because the presence of a crystal catalyzes secondary nucleation (Mersmann, 2001). Levels of supersaturation required for primary nucleation can be estimated from measurements of an induction time, which is the time taken for a supersaturated wastewater void of any struvite crystals to form a measurable number of nuclei (Mehta & Batstone, 2013). In such cases, a higher level of supersaturation generally decreases the measured induction time. However, the presence of struvite crystals is often ubiquitous around WWTPs, especially in the sludge line (see further below). Thus, secondary nucleation is expected to be the most important nucleation mechanism in industrial struvite reactors.

Once crystals have nucleated they can grow, either as single crystals by layered growth, or by aggregation with multiple crystals then forming interparticle bridges and growing together as combined crystal masses, termed agglomeration growth. Agglomeration growth has been suggested to be important for struvite precipitation in commercial systems (Galbraith *et al.*, 2014). Crystal growth rate generally increases with an increasing level of supersaturation (Mersmann, 2001).

Struvite crystal morphology is controlled by crystal growth which is predominantly influenced by the extent of supersaturation. Specifically, dendritic, fibrous and irregular crystals are favored under conditions of high supersaturation (Figure 10.10). The concentration of ammoniacal N also has an effect with more irregular crystal morphologies resulting from higher ammoniacal N concentrations with increased supersaturation (Figure 10.10) (Shaddel *et al.*, 2019). An increase in pH promotes a shift from Zone 1 to Zone 3-type crystals (Figure 10.10) (Shaddel *et al.*, 2019). Factors affecting struvite aggregation have also been researched due to their impact on struvite yield (Le Corre, 2006; Shaddel *et al.*, 2019).

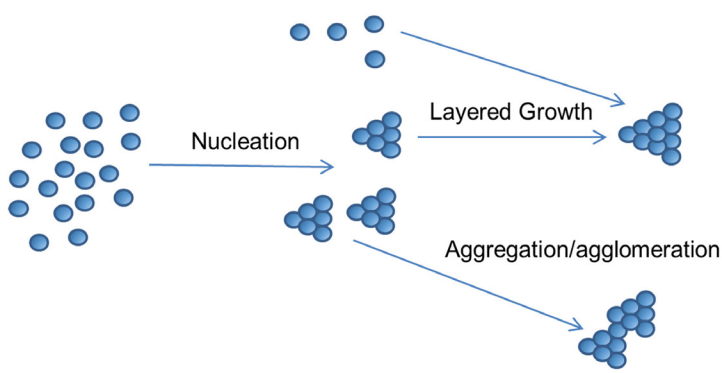

Figure 10.9 Crystal nucleation and growth processes.

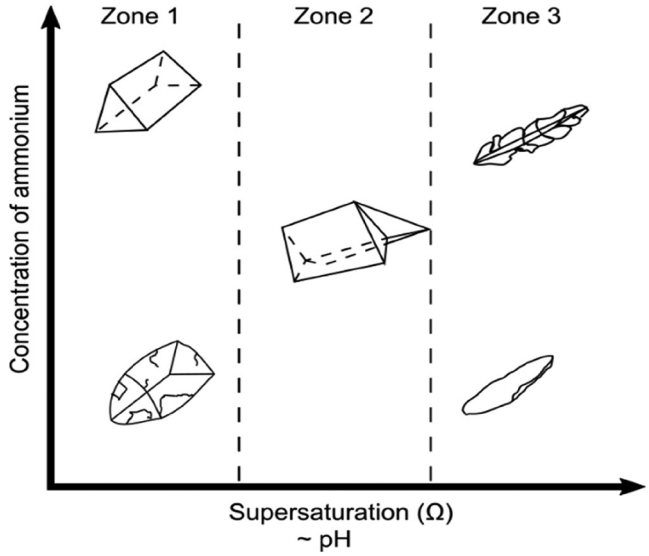

Figure 10.10 Impacts of varying supersaturation, ammonia and pH on struvite crystal morphology (adapted from Shaddel *et al.* (2019)).

Struvite crystal size is also important from an application perspective. Specifically, larger struvite crystals may be favorable for fertilizers due to ease of handling, transportation, and application (Li *et al.*, 2019a). However, the surface area/volume ratio may also be important as this would influence dissolution in soils and thus nutrient release properties (Li *et al.*, 2019a, 2019b) in fertilizer applications.

Overall, to control struvite crystal size, nucleation and particle growth processes have to be balanced by controlling levels of supersaturation in industrial processes. Specifically, a higher initial supersaturation may increase nucleation rate and produce several small particles that grow rapidly to quench the remaining supersaturation (Shaddel *et al.*, 2019). In contrast, a slow nucleation rate combined with a moderate crystal growth rate may produce a crystal product with a larger size. Some struvite precipitation processes use seed materials to promote struvite precipitation to increase particle size and improve the product purity (Le Corre *et al.*, 2009; Li *et al.*, 2019a, 2019b). Other reactor systems are designed to control supersaturation in various compartments of the precipitation reactor (see further below), to control nucleation and growth processes. The mass-based struvite formation rate (r_{cryst}, moles per L per h) which includes nucleation and growth, has been reliably represented in wastewater treatment process models by a rate expression (Mbamba *et al.*, 2015, Equation (10.13)):

$$r_{cryst} = k_{cryst} \cdot X_{cryst} \cdot \left(\left(\frac{IAP_{struv}}{K_{sp,struv}} \right)^{1/3} - 1 \right)^{3} \tag{10.13}$$

where k_{cryst} is an empirical rate coefficient (with units of per h) and X_{cryst} is struvite crystal concentration (with units of moles/L). This shows that struvite precipitation rate is catalyzed by the presence of struvite mineral phase. This can be used favorably for struvite reactor design and operation. For example, if magnesium/alkali reagent and/or raw water feed can be added in regions of a struvite reactor with high struvite crystal content (e.g., a settled crystal bed at the base of a reactor, or in locations where seed crystals are added), then the supersaturation that would result can be rapidly

consumed by a fast struvite precipitation rate catalyzed by a high crystal content. This then prevents high supersaturation hotspots to minimize nucleation of poorly settleable fine crystals that would wash out and be lost with the reactor effluent.

10.3.2 Struvite precipitation – applications and design

Struvite recovery can be implemented on the sludge line of a WWTP to treat digestate or centrate produced from anaerobic digestion of sewage sludge with $P > 50$ mg/L (Figure 10.11). Within this context, N and P are accumulated in sludge which is subsequently released by hydrolysis within the anaerobic digestion stage. This results in phosphate and ammonia at concentrations well in excess of that in the water mainline of the WWTP, which is then more suitable for struvite precipitation (Sena & Hicks, 2018). Other industrial and agricultural wastewater streams have also been previously explored for P recovery by struvite precipitation, including food processing and rare-earth processing wastewaters with typically high phosphate contents (Kataki *et al.*, 2016; Ma *et al.*, 2018). High phosphate in such cases usually results from biological decay processes (e.g., manure storage) or from the addition of industrial phosphate-based chemicals.

The influent is commonly dosed with magnesium compounds, typically $MgCl_2$, $Mg(OH)_2$ or MgO, to increase supersaturation and induce struvite precipitation. The concentration of magnesium can be dosed to ensure that, stoichiometrically, to exceed a minimum molar ratio of Mg:P $\geq$ 1:1 (Le Corre *et al.*, 2009). Additionally, pH must be adjusted for most wastewater influents because municipal wastewater pH varies between 7 and 8 while optimum struvite precipitation occurs at pH $\geq$ 8.5 (Le Corre *et al.*, 2009). For increasing pH in struvite recovery processes, either the wastewater is aerated, which strips CO_2, or an alkali reagent can be dosed (i.e., NaOH or $Mg(OH)_2$). Adding NaOH to raise pH and $MgCl_2$ as magnesium source may be preferred from an operational perspective so that pH and magnesium dose can be varied independently. However, NaOH is more costly and currently less economical than alternatives for pH adjustments (Muhmood *et al.*, 2019).

Reagent dissolution of $Mg(OH)_2$ or MgO can be limited by high pH, or by the precipitation of struvite that can coat magnesium reagent particles added as a slurry to the struvite process, thereby preventing further dissolution and reaction of the magnesium reagent (Romero-Guiza *et al.*, 2015). This may increase the requirement for magnesium reagent when using $Mg(OH)_2$ or MgO. Calcium (e.g., from $Ca(OH)_2$) is an impurity that can negatively influence struvite formation and co-precipitates with phosphate as calcium phosphate minerals competing with struvite formation (Le Corre *et al.*, 2009).

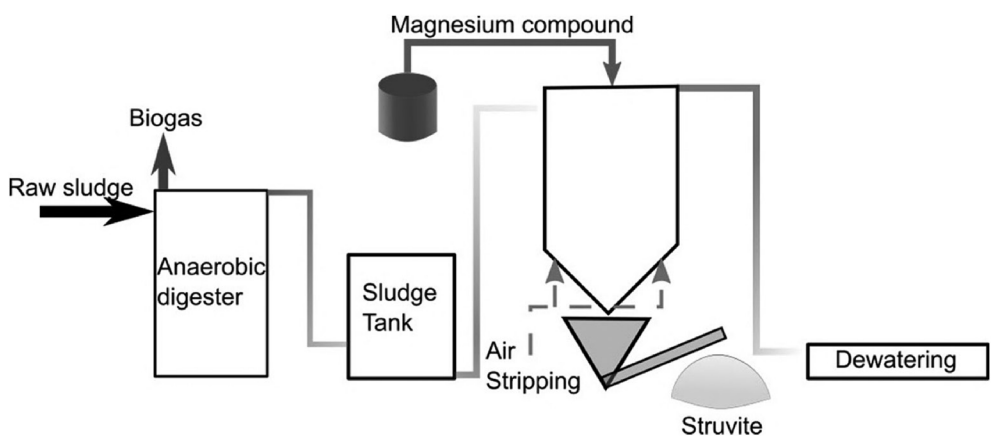

Figure 10.11 Simplified schematic of a sludge treatment section of a wastewater treatment plant with struvite precipitation.

This can especially be the case when molar ratios Mg:Ca ≥ 1:1, at which struvite formation can be limited and even inhibited (Le Corre *et al.*, 2009).

10.3.2.1 Worked exercise 1c – magnesium reagent requirements

As an illustrated example of how to determine magnesium requirements to achieve a certain desired P removal, consider the wastewater from exercise 1b at pH 7.98. The PhreeqC simulation will now precipitate struvite from this wastewater until equilibrium is attained (i.e., until $SI = 0$). To do this, struvite mineral phase is added to the model input. For this, a nominal amount of 0.01 moles of struvite is added to 1 L of wastewater in the simulation to allow PhreeqC to precipitate the struvite. Figure 10.12 shows the resulting simulation input window.

The results of the simulation are presented in Figure 10.13. Approximately 3.465×10^{-3} moles of struvite precipitated from 1 L of the wastewater (See 'Delta' for struvite under 'Phase assemblage') until equilibrium was attained. As a result of struvite precipitation, wastewater pH had also decreased from 7.98 to 7.14. This is expected and is a result of the removal of NH_4^+ and PO_4^{-3} which initiates a flow-on effect on ion pairs in the wastewater to overall liberate a net amount of H+ into the wastewater and thereby decrease the wastewater pH. Consequently, struvite processes may have an on-going alkali demand to maintain an elevated pH for struvite precipitation to continue. The results also show that total P content had decreased from 6.483×10^{-3} molal (200 mg/L) to 3.020×10^{-3} molal (~94 mg/L), or a P removal/recovery of 53% was achieved. It is also apparent that the residual magnesium concentration after struvite precipitation has now decreased to a negligible

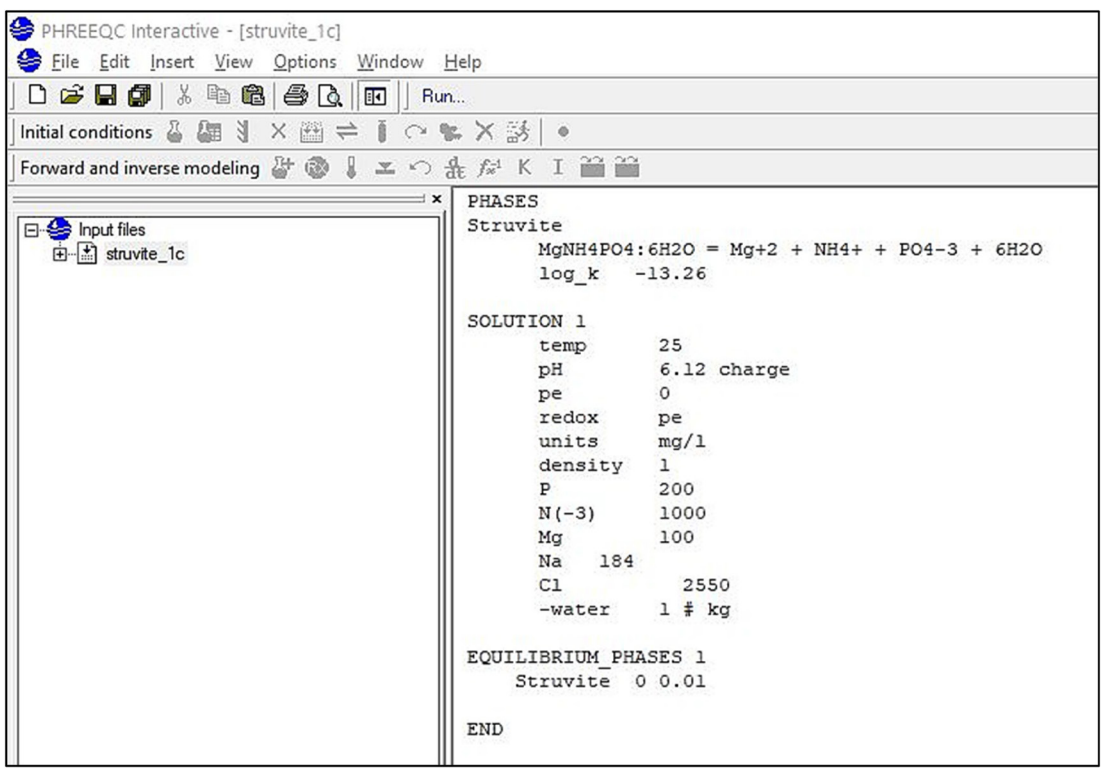

Figure 10.12 Simulation coding window (input) for PhreeqC simulation – Exercise 1c.

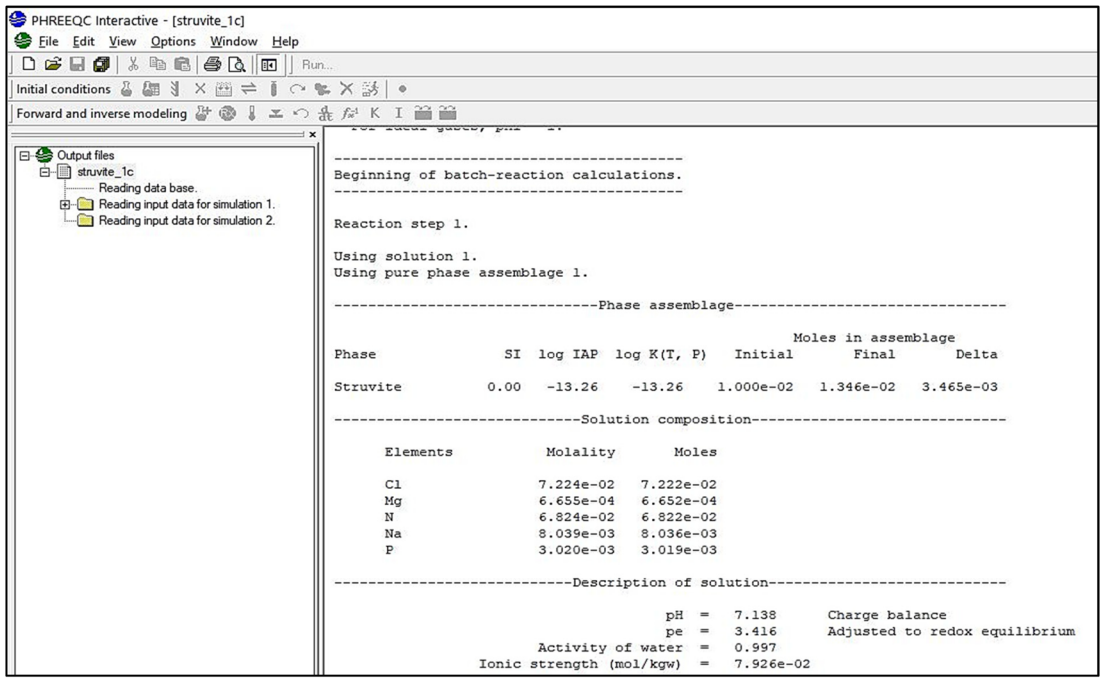

Figure 10.13 Simulation results for PhreeqC simulation – Exercise 1c.

6.655×10^{-4} molal (~16 mg/L), whilst ammoniacal N content had reduced comparatively little, down to 6.824×10^{-2} molal (~955 mg/L). This indicates that magnesium is the limiting reagent and that ammoniacal N was in large molar stoichiometric excess for struvite formation, as is typical for many wastewaters, including in the sludge line of a WWTP. This is why a magnesium reagent is often needed to increase P recovery as struvite, and also why the extent of N removal by struvite precipitation is typically low (Mehta *et al.*, 2015) unless a phosphate source is added to instead target N removal (Li *et al.*, 2019a, 2019b).

To achieve the desired >85% P recovery, the mineral Brucite ($Mg(OH)_2$) could be added to the simulation together with struvite. This can be done under the Phases 'Equilibrium_Phases' tab, or can be typed directly into the simulation command window as follows:

```
EQUILIBRIUM_PHASES 1
   Struvite 0 0.01
   Brucite 0 0.002
```

When the simulation is then rerun with this amount of brucite added, the final pH after struvite precipitation is 7.66 and the final P is 8.36×10^{-4} molal (~26 mg/L). Alternatively, magnesium chloride could be set up as a highly soluble phase (a nominal very large log_k value) as follows:

```
PHASES
Magnesium_chloride
      MgCl2 = Mg+2 + 2Cl-
log_k 100 000 000
```

and a separate alkali such as sodium hydroxide set-up:

```
PHASES
Sodium_hydroxide
        NaOH = Na+ + OH-
log_k 100 000 000
```

and a combination of these added to the simulation, instead of Brucite, until the desired 85% P removal is achieved.

In addition to the chemical requirements to control the stiochiometry and yield of struvite recovery, other process design features are implemented to achieve better control of formation and separation of struvite crystals. For this, it is important to prevent supersaturation hotspots and excessive nucleation while still promoting precipitation growth. Chemical reagents responsible for increasing/maintaining supersaturation may hence be added:

- directly into a well-mixed reaction zone together with fresh influent and a high struvite crystal concentration; or
- into areas of a reactor where there are low residual phosphate concentrations with a subsequent recycle to a well-mixed reaction zone where fresh influent is added and a high crystal content is present.

In addition, commercial designs incorporate these important features of precipitation/reaction, and also settling separation in different ways by altering:

- the hydraulic design of the reactor, for example to promote high flow in certain parts of a reactor with homogeneous mixing, and to slow down flow in other parts of the reactor to allow settling-separation of struvite crystals;
- the operational parameters, such as agitation speed, flowrate of a fluidization medium (gas or liquid), or influent flow rate;
- by varying the location and amount of chemicals added; and
- controlling pH.

These features would influence the construction costs of the struvite reactor, and also operational costs, such as energy costs and chemical costs.

Particle settling separation aims to retain fine struvite crystals so that they do not wash out with the effluent, and grow into a desired coarse crystal product. In struvite crystallizers, this settling can be achieved either with an inbuilt settling zone or an external settling tank that is separate to the struvite reactor. It is important to note that settling of particles in a bed of crystals can transition from free settling at a low solids concentration (e.g., Stoke's law) to hindered settling at a high solids concentration. Fluid up-flow velocity is also important and the various fluidization regimes are illustrated below (Figure 10.14).

The most common configurations of struvite recovery systems are: (i) fluidized bed reactors (FBR); and (ii) continuously stirred tank reactors (CSTR) (Li *et al.*, 2019a, 2019b). FBR is a continuous process where fresh influent is constantly pumped into the reactor to fluidize the struvite crystals to grow (Figure 10.15), whereas CSTR are typically operated in batch or semi-continuous mode with mechanical stirring (Figure 10.16). Reported phosphate recovery processes using struvite are summarized in Table 10.1.

The basic principles of the FBR design and operation include: constant influent flow, sometimes including return effluent to maintain fluid velocity when influent rate fluctuates (Figure 10.15) to maintain up-flow velocity in a reaction zone; and establishing supersaturated conditions within the reaction zone to promote struvite precipitation (Figure 10.15). Crystals will continue to grow until their settling velocity exceeds the up-flow velocity of the FBR (Figure 10.15). The precipitate can then

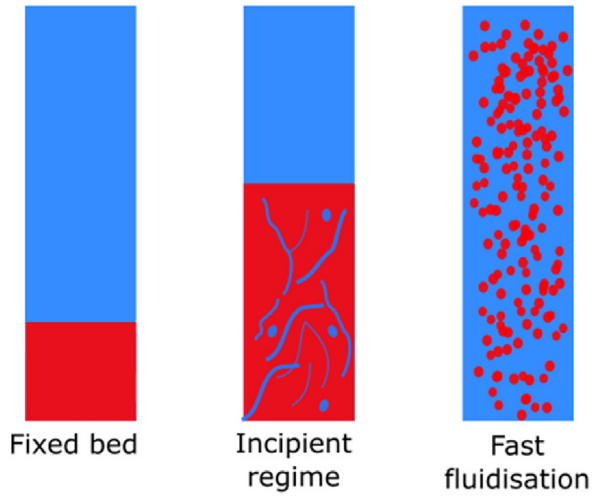

Figure 10.14 Fluidization regimes as a function of fluid velocity (adapted from University of Florida (2015)).

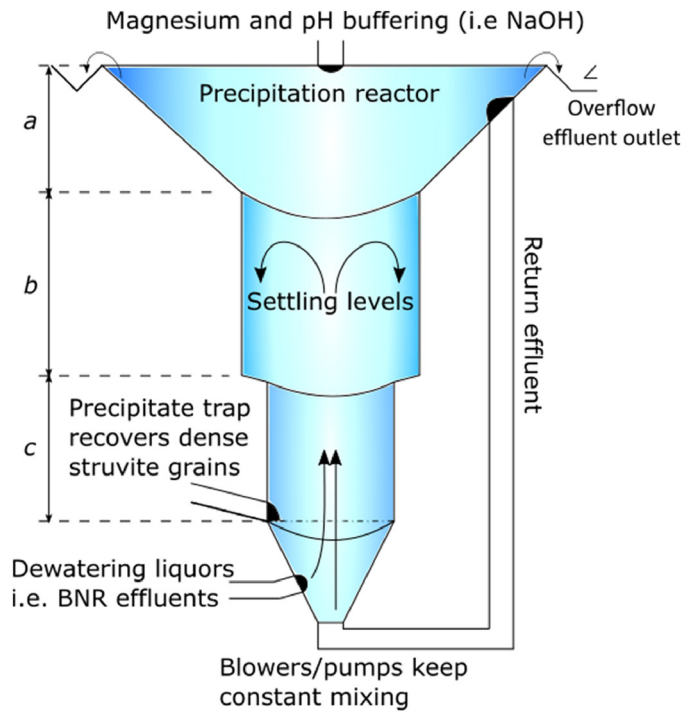

Figure 10.15 Schematic representation of a fluidized bed reactor (FBR), where dewatering liquors from a Biological Nutrient Removal (BNR) wastewater treatment plant is pumped at a constant flow into the bottom of the reactor and mixed with return effluent. Zone a = mixing and struvite reaction zone, nucleated struvite settles into zones b and c = struvite growth/aggregation zone and collection.

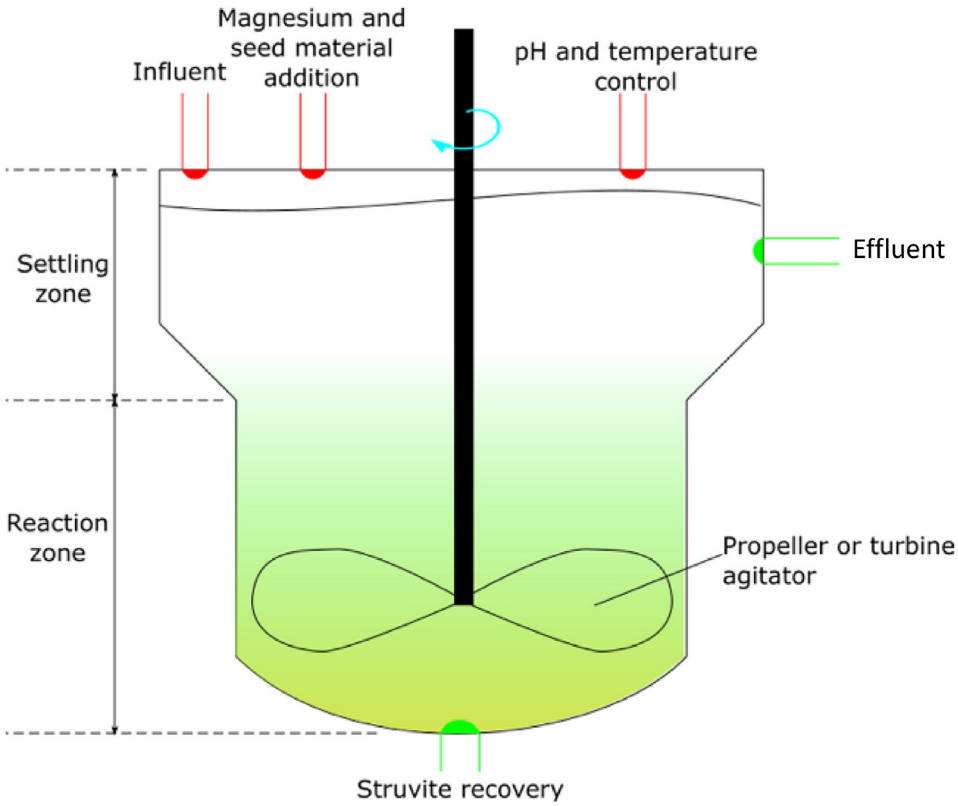

Figure 10.16 Schematic representation of a continuous stirred tank reactor (CSTR) design for struvite recovery in WWTPs.

be recovered from the base of the FBR using a mesh guard, dewatered, and dried for reuse (Figure 10.15). Ostara's Pearl© technology and Royal Haskoning DHV's Crystalactor® technology utilizes FBR struvite recovery at municipal WWTPs across the globe (Table 10.1). The Pearl© process also uses sand grains to seed struvite nucleation and ensure concentric growth to produce more aesthetic struvite that are easier to separate via settling and have properties that allow for direct application after drying of the recovered product.

The settling of a bed of struvite crystals in a FBR can help detach the solids/crystal retention time from the hydraulic retention time, so that crystals can be harvested in batch, whilst the liquid throughput occurs continuously (Le Corre *et al.*, 2009). The time constant for struvite precipitation in terms of phosphate removal appears to be in the order of hours (Mbamba *et al.*, 2015) rather than days as for biological processes. Hydraulic retention times can be as short as 1–2 hours (Munch & Barr, 2001). Simoes *et al.* (2018) suggested retention times for chemical struvite precipitation in FBRs to be in the range of 0.5–9 hours based on the cited literature studies of Ueno and Fujii (2001) and Le Corre *et al.* (2009). This indicates that a reasonable hydraulic retention time could be around 2 hours. The crystal retention time, in contrast, has to be much longer, in the order of days (Le Corre *et al.*, 2009). For example, around 10 days was required to allow sufficient time for growth of 0.5–1.0 mm struvite pellets (Ueno & Fujii, 2001). Similar results were noted by Le Corre *et al.* (2009) from other literature studies.

Table 10.1 Examples of commercially available or demonstration-scale phosphate recovery processes at WWTP (adapted from Kataki *et al.* (2016) and European phosphate platform success stories (2019)).

Technology	Influent	Reactor Type	Treatment Process	Recovery Efficiency	First Commercial Plant	Plant Size/ Capacity	Yields	Website (Where Applicable)
Pearl© Technology	Municipal wastewater	FBR	Side stream treatment of dewatering liquors via $MgCl_2$ and NaOH addition	80% P-PO_4, 10–15% N	2009, WWTP Oregon, USA	80 mg P/L, 600 000 PE	600 ton *Crystal Green*® struvite/ year	http://www.ostara.com
Crystalactor©	Municipal and industrial wastewater	FBR	Side stream treatment of dewatering liquors via $MgCl_2$, Aeration for stripping CO_2, or lime addition. Quartz sand for seeding	70–80% P-PO_4	1994, Edam Geestmerambacht, Netherlands WWTP	230 000 PE		https://www.royalhaskoningdhv.com/en/crystalactor/about-crystalactor
Phospaq™ and Anammox®	Food processing and municipal wastewater	CSTR	Aeration, stripping CO_2, increasing pH and adding MgO	80% P-PO_4, 90% N-NH_4	2011, Waterstromen-Aviko	260 kg P/L 160 000 PE	400 ton struvite/ year	https://en.paques.nl/
Struvia™	Agricultural and municipal wastewater	CSTR Turbomix™	Dosing of Mg-salts, NaOH buffers pH 8–9. Rapid mixing	80–90% P-PO_4	2016, Helsingør Denmark	250 mg P/L 72 000 PE	110 kg struvite/day	https://www.veoliawatertechnologies.com/en/solutions/products/struvia
AirPrex™	Sewage sludge (SS)	FBR air lift reactor	Aeration of digested sludge removes CO_2 and increases pH. Dosing of Mg-salts	90–95% P removal	2009, MG-Neuwerk, Niersverband, Germany	995 000	1000 kg struvite/day	www.p-rex.eu

Multiform	AD sludge dewatering liquors	FBR	Dosing of $MgCl_2$ and NaOH	80% PO_4, 20% N	2012, Idaho USA			www.multiformharvest.com
Polonite® and Sorbulite® filter beds	Agricultural wastewater	Granulated beds	Filtration over CaO. SiO_2, $CaSiO_3$ (polonite®) granules, P-precipitation nucleates around granules	100 mg P/g of Polonite®	4000 + farmsteads in Sweden since 2010		Reclaimed granules are slow release fertilizers	
Seaborne	AD effluents/SS	CSTR	Acidification to separate heavy metals and P, struvite precipitation using $Mg(OH)_2$ and NaOH		2007, Gifhorn WWTP, Germany	50 000 PE	250 kg struvite/day and heavy metals	
RecoPhos (electro-chemical)	Sewage sludge ash (SSA)	Electro-thermal reactor	SSA put into electrothermal carbon packed bed at 1300°C. P is volatized and distilled into acid. Molten slag collected	Up to 100% P from ash			RecoPhos® P38fertilizer or H_2PO_5 Fe-melt	RecoPhos (2012) http://www.recophos.org/
AMS Technologies	SSA	CSTR	Acidification, leachate filtered to remove suspended solids. Nanomembranes retain heavy metals	Up to 60% P as H_3PO_4			Recycled heavy metals, phosphoric acid	Paltrinieri *et al.*, (2019), http://www.amsmembrane.com/index.php/en/applications/acids

PE – population equivalent.

In a CSTR crystallization reactor, pH modification takes place through the addition of an alkaline chemical, and propeller or turbine mixing is provided within the reactor (Figure 10.16). Baffles are added to prevent the formation of vortices which could be detrimental to crystal growth. Turbines create a radial flow, causing intensive turbulence and increased fluid shearing to produce finer precipitates, which can be desirable in some cases (Regy *et al.*, 2001).

The Struvia™ process is an example of a CSTR based technology for struvite recovery (Table 10.1) (Brockmann, 2015). The process treats nutrient-rich effluents from industries or dewatering sludge liquors. The CSTR includes a proprietary mixing technology (Turbomix®) and a lamella settler. The influent is first mixed, dosed with magnesium salts, buffered to pH 8–9 and then passed through the enhanced mixing system. The latter encourages crystal formation and growth, reduces reaction time and improves the efficiency of chemicals added. The integrated lamella settler ensures the separation of the produced struvite and the treated effluent that is returned to the head of the WWTP works. The collected struvite is then dried and processed into organo-mineral fertilizers for agricultural use.

10.3.3 Struvite precipitation – case studies of full scale implementation

Currently, there are an estimated 80 struvite precipitation installations in operation worldwide (Muys *et al.*, 2021). This section provides three case studies, showing different reactor configurations and process features.

10.3.3.1 Case study 1 – ostara®'s pearl©

Ostara®'s Pearl© nutrient recovery system is a modular process made by Ostara Nutrient Recovery Technologies Inc. (Vancouver, Canada). The process is adaptable to different nutrient-rich streams (e.g., sewage sludge liquors, streams from food processing). The wastewater to be treated is first dosed with Mg, circulated in a fluidized crystal forming reactor, with the pH strictly controlled using NaOH (Table 10.1). To initiate crystallization, small struvite crystals act as seeds to ensure that the precipitates grow into granules, fit for distribution after drying. This can be achieved by recycling into the reactor treated effluent with uncollected struvite crystals. Fluidization of the bed is achieved by a recycle, which is responsible for maintaining a constant upward velocity in the reactor regardless of the feed flow. Ostara® markets these granules as Crystal Green® (Figure 10.17), an aesthetic product designed to improve consumer confidence in recovered nutrient fertilizers.

Figure 10.17 Ostara® struvite granules commercialized as Crystal Green® Ostara pearls (left) and Pearl© Technology reactor (right).

Ostara operates at different WWTPs in Europe, including Madrid El Canal Isabell II WWTP (FuturEnviro, 2017). The nutrient recovery facility consists of two groups of feed pumps, a crystallizing reactor and its associated pumps and valves, a draining and drying product step, a product sorting and packaging step, a programmable logic controller (PLC) cabinet, an engine control centre, an $MgCl_2$ storage tank and an NaOH storage tank. The anaerobic digested sludge and the overflows of the dehydration and the flotation tanks are fed into the lower part of the reactor where they are diluted with recirculation water and $MgCl_2$ (32%; 100 L/h) and NaOH (25%; 36 L/h) are injected. Inside the reactor, the struvite precipitates in a controlled way in small hard granules. At the top of the reactor, an integrated clarifier retains the granules inside the reactor. The effluent is sent to a tank from where it is pumped to the primary decantation of the WWTP. Struvite particles are collected from the bottom of the reactor, washed, dried, sorted by size and packaged for shipment.

Struvite formation rate and its physical properties are controlled in the process so that a high-quality product is obtained, which allows it to be marketed as a fertilizer. The struvite recovery system is designed to recover phosphate from a combined feed, in the range of 50–120 m^3/h maximum anaerobically digested sludge, dehydration overflows, and flotation overflows. The reactor is designed to treat a maximum precipitable P load of 300 kg/day. The installed reactor allows production of up to 2 tons/day of marketable final product, called Crystal Green®. Under optimum operating conditions and feed quality, 600–700 tons can be produced per year.

10.3.3.2 Case study 2 – Airprex®

A variation of the FBR design uses an airlift system to achieve air stripping of CO_2 and thus increase operational pH, and also to provide mixing. An example is the Airprex® process developed by Berliner Wasserbetriebe (BWB) in cooperation with Technische Universität Berlin, which has been installed to treat a range of anaerobic digestion effluents. Magnesium is added as $MgCl_2$ and the airlift design allows for the digestate to flow upwards in the central compartment of the reactor inside a draft tube, and down via the annulus region by the downdraft of fluid (Figure 10.18).

Pumping air has a significant energy demand and costs, but the process has been demonstrated to be attractive due to savings in pH adjustment chemicals and from not requiring dewatering,

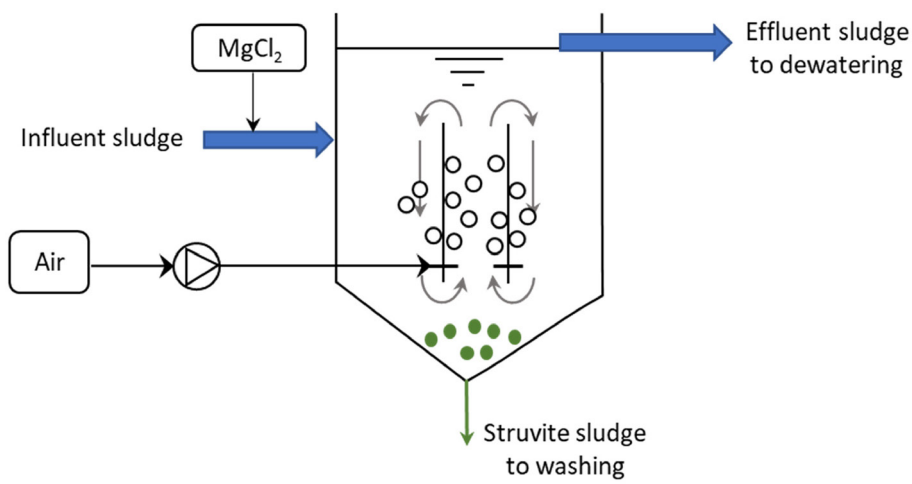

Figure 10.18 Air-lift arrangement of the Airprex® process which both provides mixing as well as CO_2 stripping to elevate pH and save on alkali dosing (adapted from P-Rex (2015)).

because P is recoverable directly from digestate with this process, and not from a centrate. The struvite product can be crystallized within the wet sludge and hence contains organic and inorganic impurities. The formed struvite crystals are harvested at the bottom of the reactor. This is done a few times per day by opening the bottom of the reactor for a minute or two and a mixture of organic material and struvite crystals is released to a pump, which delivers it to a washing system that dislodges the organics by floating it to the top of the washer to be decanted back to the treatment plant headworks.

The largest Airprex operational plant is located in Berliner Wasserbetriebe in Germany with a capacity of 2000 m^3/day of digested sludge, with struvite production of 2.3 ton/day. The AirPrex® process was said to be the first process that recovered products recognised as fertilizers, by achieving the official conformity approval and REACH registration. The application of the process is said to be limited to WWTPs with enhanced biological P removal and P concentrations >50 mg/L PO_4-P in the sludge liquor, even though the product yield can be enhanced by thermal or chemical hydrolysis prior to digestion to increase P concentration in the sludge digestate (P-Rex, 2015).

10.3.3.3 Case study 3 – Phospaq™

Stoke Bardolph WWTP in the UK serves a population equivalent of approximately 650 000 and has a unique range of technologies for sludge and centrate treatment, including the BIOPAQ® UASB for methane production combined with nutrient management, including struvite recovery, through the Phospaq™ process and N abatement using Anammox® (Table 10.1, Figure 10.19). The Anammox® promotes BNR in sludge dewatering liquors through deammonification. The deammonificaion process effluent is then treated by the Phospaq™ process.

The effluent from the Anammox® process is then aerated in two Phospaq™ struvite reactors (stripping CO_2 and increasing pH). The influent is dosed with magnesium oxide (MgO) to promote the precipitation of struvite. In addition to struvite removal, aeration increases the availability of oxygen for biological reduction of COD. The recovered struvite can be directly applied to land after drying. The Phospaq™ struvite reactors are equipped with separators that can retain the struvite to be harvested from the base of each reactor.

The Phospaq™ is said to be feasible for applications with P loadings of more than 100 kg P/d and P concentrations of 50 mg/L PO_4-P or more and N concentrations of 200 mg/L NH_4-N or more, and can achieve a removal efficiency of about 70–95% (www.paques.com).

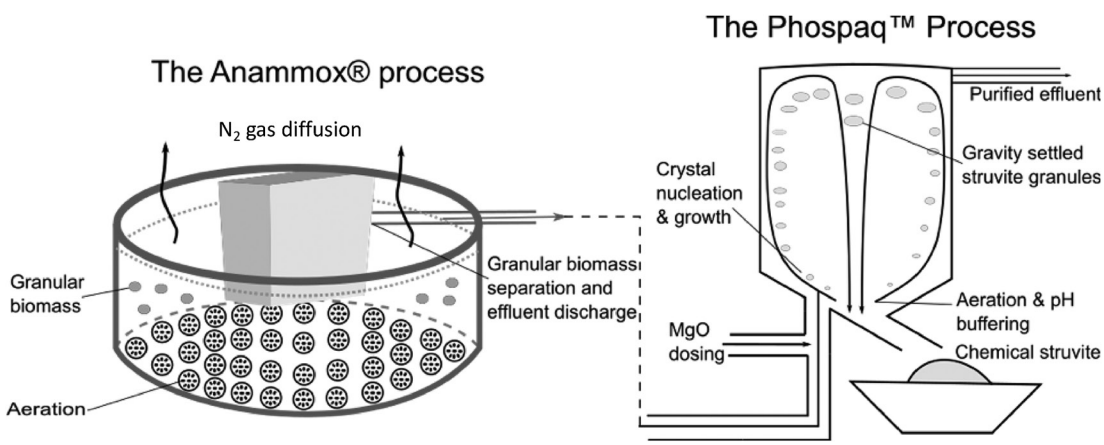

Figure 10.19 Combined Anammox® and Phospaq™ system (adapted from www.paques.com).

10.3.4 Struvite precipitation – challenges, opportunities and research needs

10.3.4.1 Struvite as a fertilizer and its value

Mined phosphate used as fertilizer is predominantly refined from the apatite group of minerals ($Ca_5(PO_4)_3$(OH, F, Cl)). In the last 10 years, almost 400 studies have been published on the effects of struvite as a fertilizer. Doyle and Parsons (2002) suggested that struvite is an excellent fertilizer, due to its low solubility and high N and P content. It has been reported that struvite is at least as effective a P source for plant nutrition as commercial mineral P fertilizers. In addition, the content of heavy metals is low compared to phosphate rock. According to Rittman (2011), struvite quality is comparable to standard fertilizers such as superphosphate and diammonium phosphate. A key factor for the management of struvite and similar recycled P sources is to increase the bioavailability and plant P-uptake efficiency (uptake per unit of root surface area) under different soil conditions. Therefore, knowing how to increase struvite P-use efficiency at different soil pH values will make its use more reliable as a substitute for rock phosphate (Robles-Aguilar *et al.*, 2019).

The current market price of struvite is estimated to be between €188 and €763 per ton. A recent study by Muys *et al.* (2021) estimated typical marketed values between €0 and €100 per ton, with some products marketed at considerably higher prices of €350 per ton (Phoshorgreen) to €1000 per ton (Pearl). Around €2–3 per kg in operational cost savings involved in P recovery can be achieved compared to conventional removal. However, Munch and Bar (2001) said that if struvite is sold as a boutique fertilizer, a conservative estimation for the selling price could be substantially higher. Chemical reagent costs strongly influence the economic feasibility of struvite recovery, which can vary significantly with wastewater composition and the type of chemicals being used (Li *et al.*, 2019a, 2019b). The cost of chemicals for pH adjustment can be greater than that for magnesium addition (Li *et al.*, 2019a, 2019b).

When considering the economic feasibility of implementing a struvite precipitation process, it is important to consider associated benefits such as: a potential to reduce the chemical dosage in traditional P removal techniques and an associated potential to reduce sludge to landfill costs (Li *et al.*, 2019a, 2019b); eutrophication prevention and an increase in the availability of a renewable P (Li *et al.*, 2019a, 2019b); and struvite deposition control around a WWTP (Li *et al.*, 2019a, 2019b). A recent review (Sena & Hicks, 2018) indicated that the environmental impacts of struvite production would be comparable to that of P removal by a conventional WWTP.

10.3.4.2 Technological and regulatory considerations

Magnesium is usually the limiting component for struvite crystallization in wastewater. The dosing of magnesium hydroxide ($Mg(OH)_2$) provides a source of magnesium and increases pH, although using $Mg(OH)_2$ can destabilize the process as discussed above (Chimenos et al., 2006; Lee *et al.*, 2003). Not withstanding process stability considerations, the most common sources of magnesium are MgO and $Mg(OH)_2$, despite their low solubility compared to $MgCl_2{\cdot}6H_2O$ and $MgSO_4{\cdot}7H_2O$. The latter are, however, more expensive.

Ammonia removal by struvite precipitation is generally low in comparison to phosphate removal because waste streams typically contain a molar excess of ammonia N (Mehta *et al.*, 2015). The molar excess ammonia then remains in soluble form and is not recovered (Mehta *et al.*, 2015), unless a phosphate source is added to specifically target ammonia removal (Li *et al.*, 2019a, 2019b), in which case ammonia removal extents of up to 99% could be achieved.

Commercialization of struvite as a fertilizer started in Japan in the year 1998 (Ueno & Fujii, 2001). Struvite is yet to be widely recognized as a fertilizer (with the exception of a few countries). However, a recent study (Muys *et al.*, 2021) sampled and analyzed struvite from 24 European production plants and showed that only three of these sampled products failed physicochemical legal limits of the revised fertilizer regulation issued by the EU in 2019. Specifically, one of the sampled products had a P content $<7\%$ and three samples exceeded the limit for organic carbon content of 3% by dry weight (Muys *et al.*, 2021). The new fertilizer regulation defines 17 physicochemical and five microbiological

parameters that a product must meet to be used as a fertilizer or as a component material in N, P, K fertilizers (Muys *et al.*, 2021).

Microbiological analyzes by the same sampling and analysis study (Muys *et al.*, 2021) indicated that struvite may exceed certain legal limits, albeit that struvite crystallization is able to selectively exclude pathogens (Muys *et al.*, 2021). The study observed that struvite recovered from digestate contained more pathogens compared to struvite from the dewatering liquor of digestate (Muys *et al.*, 2021). A gentle drying process (below the decomposition temperature for struvite) may also benefit further reduction in pathogen contamination in the product (Muys *et al.*, 2021).

10.3.4.3 Other opportunities for phosphorus recovery and research needs

While struvite remains the dominant marketed fertilizer recovered from wastewaters, the search for less reactant-intensive and less energy-intense processes for P recovery continues. One possibility is to recover phosphate as vivianite, which is an iron phosphate mineral found in hydrothermal deposits, anoxic soils and sewage sludge. It can be used in lithium ion batteries, slow-release fertilizers and has magnetic properties (Wu *et al.*, 2019). Iron reduction occurs in anaerobic digesters where sulfate and methane-reducing bacteria dominate. Reduced iron reacts with phosphate ions to form vivianite ($Fe_3(PO_4)_2.8H_2O$). Vivianite crystallizes in neutral to weak-basic pH, which removes the need for dosing wastewaters with bases as currently employed in many commercial struvite removal processes. However, high concentrations of dissolved iron are required, which pose a problem when removing vivianite crystals from the sludge without incorporating organic matter into the crystals due to the high sorbent quality of organic matter to heavy metals. Possible solutions are to use magnetic plates to remove the vivianite crystals or centrifugation (Wu *et al.*, 2019). Further research is needed to elucidate the factors influencing vivianite crystallization, to enhance its removal, and to ascertain how best to incorporate it into treatment processes.

Other strategies to add magnesium to wastewater can be considered, including the use of desalination by-products (e.g., nanofiltration of sea water) that have an adequate magnesium concentration and an appropriate Mg/Ca-ratio, (Anne *et al.*, 2001), seawater (Matsumiya *et al.*, 2000) or salt concentrate (Etter *et al.*, 2011), which can be lower cost alternatives. However, these may contain other ions which could shift chemical equilibria, negatively impact on struvite formation and crystal growth, and increase the competition between struvite and calcium minerals.

Another option may be to add lightly-calcined magnesite to wastewater effluents to release magnesium through hydrolysis at pH 8 (Wei *et al.*, 2019). The released magnesium binds with ammonium and P remaining in the effluent to form struvite. Initial feasibility analysis of the process concluded that the cost of this process is just 11% of current commercial chemical struvite recovery systems (Wei *et al.*, 2019). However, the production of light calcined magnesite requires a readily available magnesium oxide source; and calcification of the magnesium oxide requires a kiln process heating the substance between 650 and 800°C for 2 hours. These processes themselves require energy and resources.

Struvite nanowires are an exciting recovery prospect as the nanowire morphology is better suited for slow phosphate release (Li *et al.*, 2019a, 2019b) and could achieve a more positive agronomic response and greater value. This controlled crystallization method regulates sodium chloride and pH to produce struvite nanowires in synthetic wastewaters. Findings showed a more pure struvite achieved in nanowires by regulating sodium chloride at 3.5–4.5 wt% and maintaining a pH of 11 (Li *et al.*, 2019a, 2019b). However, future studies into this technology would need to address application to actual wastewater at a larger scale while balancing the costs of materials to buffer the effluent and reactants to produce struvite nanowires.

Biological crystal formation of P compounds (e.g., struvite; magnesium phosphate, etc.), has been demonstrated to be a by-product of the metabolism of specific bacteria that can be found frequently in the environment. Bio-mineral formation refers to a series of processes involving selective extraction, uptake and incorporation of elements from the local environment into functional structures under

strict biological control. Organisms can control construction and synthesis of minerals through changes in local chemistry with different shaping strategies. Compared with inorganic minerals, biominerals are often characterized by greater structural sophistication and morphological diversity, and biological functions such as structural support, mechanical strength, protection and storage. Biological struvite (bio-struvite) production has been investigated in sludge dewatering liquors and activated sludge liquors (Leng & Soares, 2018; Pratt *et al.*, 2012; Simoes *et al.*, 2018; Soares *et al.*, 2014). Laboratory scale experiments have shown that bacteria which cause the mineralization of struvite can function in pH from 7 to 10 (Simoes *et al.*, 2018). Furthermore, bacteria can successfully produce biostruvite in wastewater with phosphate concentrations <19.7 mg P/L, which is favorable compared to non-biological struvite precipitation processes. The biostruvite produced met fertilizer purities set by the European Union and heavy metal contaminants remained below directive levels (Leng & Soares, 2018). This research could improve the feasibility struvite recovery by reducing input and management costs, while maintaining the value of struvite as a fertilizer. However, these bacteria need to be tested in mixed cultures and at pilot plant scale to observe the impact competition has on biostruvite yields and whether controls are needed to ensure the right bacteria thrive which could incur unforeseen costs.

10.4 NITROGEN RECOVERY BY AMMONIA STRIPPING AND ABSORPTION

Nitrogen (N) in its reactive forms (ammonium, nitrate and nitrite) is essential for feed and food production for animals and humans (Matassa *et al.*, 2015). Current anthropogenic sources of N are predominately from chemical fixation using the Haber–Bosch process (100 Mt), with the remainder sourced from biological crop fixation (35 Mt) and atmospheric deposition in animal rearing (10 Mt) (Matassa *et al.*, 2015). This provides an almost endless source of N (as reactive ammonia) but the Haber–Bosch process is energy intensive and a significant source of greenhouse gas emissions.

On the other hand, N is an undesirable contaminant in many industrial, domestic and agricultural wastewaters. Current treatment technologies commonly aiming for destructive dissipation via nitrification/denitrification or deammonification using activated sludge processes (Erisman *et al.*, 2008) rather than N recovery. The loss of ammonia and nitrate to the receiving environment causes eutrophication, ammonia can be highly toxic to fish and other aquatic life, and N losses cause N_2O emissions.

Due to the growing demand for reactive N fertilizer and anticipated potential adverse effects, approaches have been proposed to more efficiently convert N into edible protein (Matassa *et al.*, 2015). However, technologies and practices are also required to progressively move wastewater management away from destructive N dissipation towards maximising N recovery and beneficial reuse.

Ammonia stripping and absorptive recovery (Figure 10.20) is among the commercially available and most established technologies for reactive N recovery from digestate, and other concentrated wastewaters and manure (Vaneeckhaute *et al.*, 2017). In ammonia stripping, ammonia-rich water is sparged with a gas (most commonly air), which causes mass transfer of ammonia from the wastewater to the gas phase. The ammonia in the extrant gas stream can then be recovered via condensation, absorption, or oxidation, to produce a concentrated fertilizer product (Mehta *et al.*, 2015).

One example of such a product is ammonium sulfate ($(NH_4)_2SO_4$) produced via the subsequent reaction of ammonia after being absorbed into a sulfuric acid solution. This $(NH_4)_2SO_4$ product, if commercialized, could largely offset the operational costs of ammonia recovery under optimal process conditions (Vaneeckhaute *et al.*, 2017).

Even though ammonia removal can be as high as 98% (Mehta *et al.*, 2015), commercially available processes are generally only operated at 80–90% ammonia removal to reduce operating costs (Vaneeckhaute *et al.*, 2017). Ammonia stripping has high energy and chemical requirements as further described below, and biological removal processes for ammonia such as deammonification via Anammox can often be less costly (Vaneeckhaute *et al.*, 2017). However, unlike biological

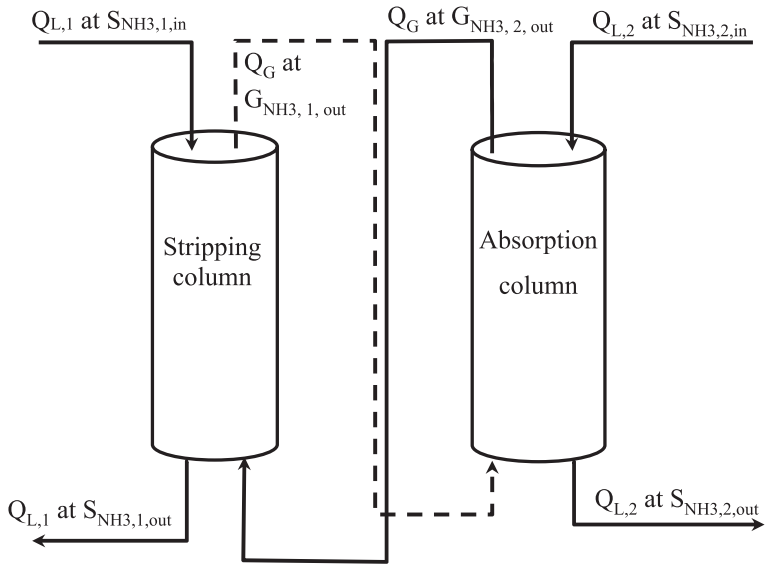

Figure 10.20 Schematic illustrating ammonia stripping and subsequent absorptive recovery, where $Q_{L,1}$ is wastewater flowrate with dissolved ammonia gas concentration of $S_{NH3,1,in}$, Q_G is gas flowrate with ammonia concentration $G_{NH3,1,out}$ (≈0).

processes, ammonia stripping recovers N, and can also remove odorous compounds and dust particles (Vaneeckhaute *et al.*, 2017). Ammonia stripping technology could thus be competitive when there is a significant commercial N-demand (Vaneeckhaute *et al.*, 2017).

In addition to producing a concentrated ammonia-based fertilizer product, ammonia recovery from wastewater and digestate can provide other benefits such as (Anaergia, 2020):

- reduced ammonia concentrations to be land-applied to meet nutrient management requirements;
- reduced potential for ammonia toxicity in anaerobic digestion of high N feedstocks; and
- reduced ammonia loads associated with returned activated sludge and centrate returned to the main water line of a WWTP for biological nutrient removal.

10.4.1 Conceptual overview – ammonia stripping and absorption

Ammonia stripping does not target N forms other than ammoniacal N, and therefore requires organic N to be mineralized into ammonia N prior to recovery. The mass transfer of ammonia from a liquid to gas (stripping), and subsequently from a gas to a liquid (absorptive recovery), is driven by a concentration driving force. This concentration driving force is the difference between dissolved (actual) ammonia concentration in the water phase ($[NH_3(aq)]$) and the solubility concentration of ammonia $[NH_3(aq)]_{eq}$ in that water if it was to be at equilibrium with the contacted gas phase, as follows:

$$N'_{NH3} = K_L a\left(\left[NH_3(aq)\right] - \left[NH_3(aq)\right]_{eq}\right) \tag{10.14}$$

where N'_{NH3} is the molar transfer rate of ammonia and $K_L a$ is the overall mass transfer coefficient defined in terms of liquid-phase concentrations.

An important concept in gas–liquid transfer is the two-film theory, where overall resistance to gas–liquid mass transfer could include a resistance to mass transfer on the gas-side of the transfer interface across a 'gas film' and separately a resistance to mass transfer on the liquid-side of the same transfer

interface across a 'liquid film' (Treybal, 1981). This leads to a relationship between an overall mass transfer coefficient $K_L a$ (as above) and the separate liquid and gas film mass transfer coefficients ($k_L a$ and $k_G a$, respectively) as follows (Treybal, 1981):

$$\frac{1}{K_L a} = \frac{1}{k_L a} + \frac{1}{K_H \cdot k_G a} \tag{10.15}$$

where K_H is the Henry's Law constant. This applies to relatively dilute liquid and gas phases at low to moderate pressures (as is the case with ammonia stripping from wastewater). The equilibrium solubility conditions described by Henry's law are as follows:

$$P_{NH3} = K_{H,NH3} \cdot \left[NH_3(aq)\right]_{eq} \tag{10.16}$$

where $K_{H,NH3}$ is the Henry's law constant for ammonia gas in water at a corresponding process temperature, and P_{NH3} is the partial pressure of ammonia in the gas phase. The units of the Henry's law constant can differ from that corresponding to Equation (10.16), for example if gas composition is defined in mole fraction instead of partial pressure.

As a result of an acid-base ion pairin water, ammoniacal N is present in two forms; ammonium ions (NH_4^+), and free ammonia (NH_3, identical to dissolved ammonia gas):

$$NH_4^+(aq) \leftrightarrow NH_3(aq) + H^+(aq) \tag{10.17}$$

Importantly, only NH_3 participates in gas–liquid mass transfer, not NH_4^+. The proportion of total ammoniacal N [that is $NH_3(aq) + NH_4^+(aq)$] that is NH_3 is influenced by pH according to the following relationship:

$$\frac{\left[NH_3(aq)\right]}{\left(\left[NH_3(aq)\right] + \left[NH_4^+(aq)\right]\right)} \times 100 = \frac{K_{NH4+} \cdot \gamma_{NH4+}}{\left(K_{NH4+} \cdot \gamma_{NH4+} + 10^{-pH} \cdot \gamma_{NH3}\right)} \times 100 \tag{10.18}$$

The value of K_{NH4+} ($= 10^{-9.252}$) for the reaction in Equation (10.17) is affected by temperature, and this effect of temperature can be empirically described by a van't Hoff relationship, as follows:

$$\ln\left(\frac{K(T_2)}{K(T_1)}\right) = \frac{\Delta H^0}{R}\left(\frac{1}{T_1} - \frac{1}{T_2}\right) \tag{10.19}$$

which relates the equilibrium constants $K(T_1)$ and $K(T_2)$ at two temperatures T_1 and T_2 in degrees K, respectively, and where R is the universal gas law constant (8.3145×10^{-3} kJ per mol per K), and ΔH^0 is the standard enthalpy of reaction (52.22 kJ per mol for the reaction in Equation (10.17) at 298 K).

The resulting ion pairing effects can also be calculated at various pH and temperature values using PhreeqC (see section 10.3.1) with the following code:

```
SOLUTION 1
temp 25
pH 8
pe 4
redox pe
units mg/L
density 1
N(-3) 1000
Cl 0.01 charge
- water 1 # kg
```

Note in this code that the simulation is set to balance ionic charge in the water by altering the concentration of a nominal inert counter-ion, in this case chloride, to ensure that the simulation correctly aligns its calculations with the nominally set pH value. To visualize the effects, the values of γ_{NH4+} and γ_{NH3} were nominally set equal to unity, and the resulting proportions of NH_3(aq) calculated using Equation (10.18) with temperature corrections via Equation (10.19). The results are presented in Figure 10.21, showing that the proportion of NH_3(aq) increases at elevated temperature and elevated pH. This is important for ammonia stripping because the efficiency of stripping relies on ammoniacal N being predominately present as NH_3(aq). The stripping unit is typically operated at an elevated pH of between 10.8 and 11.5 (United States Environmental Protection Agency, 2000). While chemical pH adjustment can be used, a potentially efficient means to elevate pH of anaerobic digestate is to pre-sparge with air to strip off dissolved carbon dioxide (CO_2), and because CO_2 is a weak acid, its removal causes a pH rise. The extent to which pH can be elevated in this way depends on background alkalinity (Vaneeckhaute *et al.*, 2017). Alternatively, it may be possible to elevate temperature using waste heat if available from onsite engine generators running on biogas from anaerobic digestion.

If ammonium sulfate is produced by scrubbing, with sulfuric acid solution used as the extractant liquid, the acidic pH conditions will rapidly convert any NH_3 extracted from the gas phase into NH_4+. This then keeps the concentration of NH_3 in the liquid phase low and encourages efficient mass transfer from the gas phase to the liquid phase. The final product can be concentrated up to 38%, yielding a liquid fertilizer of 8-0-0-9 (mass%) as N-P-K-S, and can be further crystallized and dried to yield a dry prilled fertilizer with an analysis of 21-0-0-24 (mass%) as N-P-K-S. The ammonium sulfate crystallization reaction is as follows:

$$2NH_4^+(aq) + SO_4^{-2}(aq) \rightarrow (NH_4)_2 SO_4(s) \tag{10.20}$$

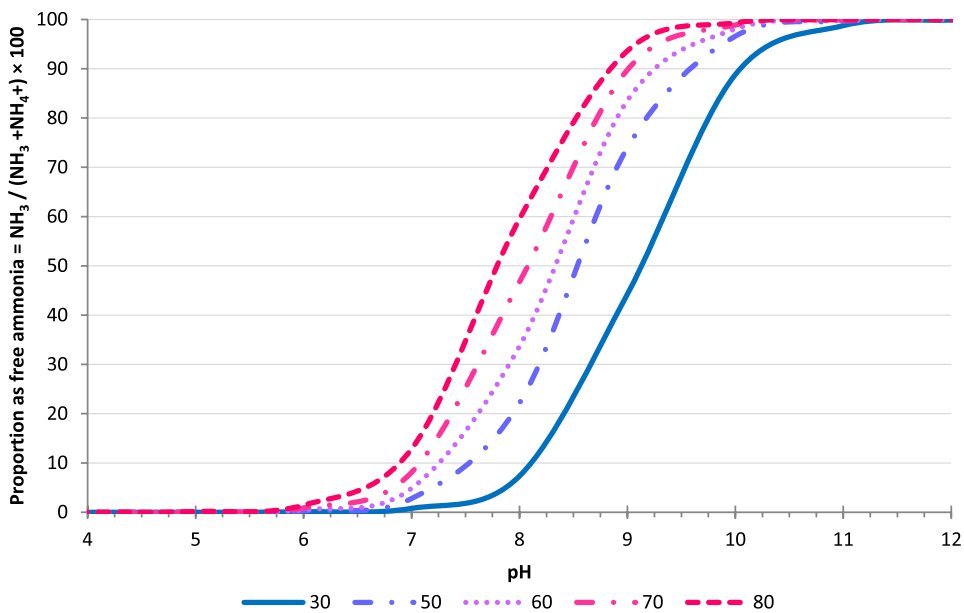

Figure 10.21 Proportion of ammoniacal nitrogen as free ammonia (NH_3), as a function of wastewater pH and operating temperature (°C).

10.4.2 Ammonia stripping and absorption – applications and design

While several possible process configurations could provide the close gas–liquid contact necessary for ammonia stripping and absorption (including plate, spray and bubble columns, and agitated vessels), ammonia stripping processes to date have mostly used packed columns (Vaneeckhaute *et al.*, 2017). Other than packed columns using structured or random packing, columns can instead be fitted with sieve plates or bubble cap trays to provide the close contact between the gas and liquid phases. In these cases the column is not liquid-filled, but is instead operated to limit pressure drop to gas flow, to prevent flooding of the column with liquid or carryover of the liquid into the gas stream (i.e., entrainment), and to ensure that liquid flow is distributed as evenly as possible across the path of the gas flow. In the case of packed columns applied to anaerobic digestate, the main technical challenge to date has been scaling and fouling of the packing material, and the resulting high energy and chemical requirements, such as for lime softening (Vaneeckhaute *et al.*, 2017). Carbonate scale formation can also be an issue, and this could be reduced with prior stripping of CO_2 (Vaneeckhaute *et al.*, 2017). This has the added benefit of saving chemicals required to raise pH to increase the fraction of NH_3 (Figure 10.21).

The tendency for minerals to precipitate (including struvite and other calcium and magnesium minerals) can be evaluated using the saturation index approaches described in section 10.3. A preceding solid–liquid separation step may be required with a packed column stripping unit to remove the majority of suspended solids that may cause clogging or fouling (Vaneeckhaute *et al.*, 2017).

Liquid-filled systems with submerged diffused gas sparging (e.g., Anaergia (2016)) on the other hand have no trays, sieves, loose media or packing that may clog or foul. As such, liquid-filled sparged reactors can be operated at higher total solids concentrations that are common in anaerobic digestion processes (e.g., 8–9% total suspended solids, (Vaneeckhaute *et al.*, 2017)) without requiring prior solids separation. However, diffused gas sparging systems tend to be less efficient than packed or low-profile tray columns (Mead & Leibbert, 1998). The height of the sparged reactor could be limited by power consumption to supply the extractant gas at a pressure above the hydraulic head at the base of the liquid-filled reactor (~1.5–2 meters). The mass transfer area in such systems would be dictated by bubble size, requiring fine bubbles to increase transfer surface area. The gas sparging system may have fine pores prone to clogging (Crittenden *et al.*, 2005) which would lead to subsequent performance decline.

For all ammonia stripping systems, demisters (mist eliminators) may be required at the top of the unit on the gas outlet to prevent liquid droplets being entrained in the exiting gas (Crittenden *et al.*, 2005).

10.4.2.1 Packed column systems

In packed columns, the gas can flow perpendicular (side-to-side) to the liquid flow (usually down), or the gas flows can flow up the column in a counter-current direction to the water or liquid extractant flowing down the column (United States Environmental Protection Agency, 2000). Commercial software packages are available for use by column suppliers to design packed, tray, or plate columns, but here the underlying analytical approaches will be presented for packed column design, because packed columns are most commonly used. The design approach for cross-flow and counter-current flow is similar, so the approach for counter-current flow will be demonstrated.

The first step in performing a preliminary design is to select an appropriate value for the stripping factor (S) defined as follows (Crittenden *et al.*, 2005):

$$S = \left(\frac{Q_G / Q_L}{1/K_H} \right) \tag{10.21}$$

with K_H in this case being dimensionless and Q_G and Q_L being the volumetric extractant gas and water/wastewater flows, each with units of m^3/s, so that S is dimensionless.

The S value indicates a minimum gas-to-water ratio for high treatment efficiencies. If $S < 1$, the stripper will be equilibrium limited and unable to achieve a high degree of removal, whilst at $S = 1$,

the operation is at the minimum gas-to-water ratio required for stripping and a high degree of removal (Crittenden *et al.*, 2005). Thus, S should be >1.

A reasonable starting value is $S = 3.5$ for many systems (Crittenden *et al.*, 2005). The gas volumetric flow (Q_G) can be calculated by Equation (10.22) for the selected value of S:

$$Q_G = \frac{Q_L \cdot S}{K_H} \tag{10.22}$$

Calculations of packed column diameter can then use a generalized Eckert pressure drop correlation plot, as shown in Figure 10.22. The Eckert plot represents empirical correlations that describe the pressure drop to gas flow through the packed column as a function of gas mass flow normalized with respect to column projected surface area (G_m, with units kg/(m^2.s)) up to a limit representing the flooding point.

To size the diameter of the packed column, the value on the horizontal axis of the Eckert plot (x) is calculated as follows:

$$x = \frac{L_m}{G_m}\left(\frac{\rho_g}{\rho_l - \rho_g}\right)^{0.5} \tag{10.23}$$

where ρ_l and ρ_g are the respective gas and liquid densities with units of kg/m^3, and L_m is the water mass loading rate normalized with respect to the column projected surface area (kg/(m^2·s). The ratio of L_m and G_m can be calculated from the ratio of Q_G and Q_L as follows:

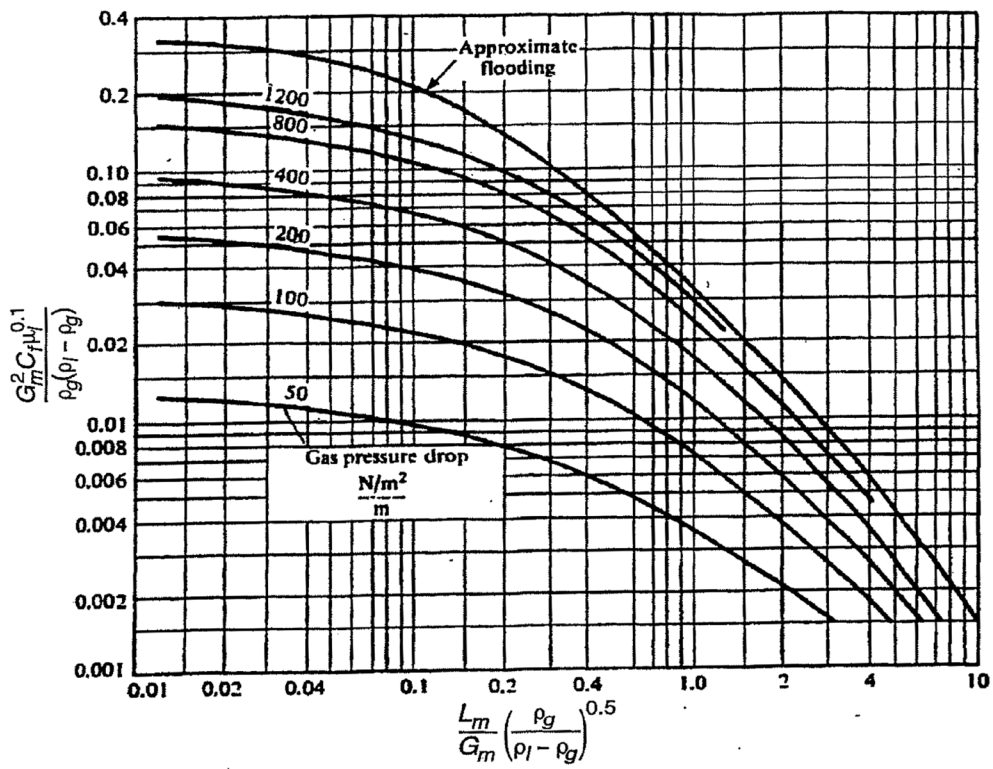

Figure 10.22 Generalised Eckert correlation plot for a random packing tower (Sourced from Crittenden *et al.* (2005) and (Eckert, 1961; Treybal, 1981) cited therein).

$$\frac{L_m}{G_m} = \left(\frac{Q_L}{Q_G}\right) \cdot \left(\frac{\rho_L}{\rho_G}\right) \tag{10.24}$$

Selecting a suitable nominal pressure drop to gas flow, the corresponding value on the vertical axis of the Eckert plot (y) is then read off and the value of G_m is calculated from the following formula:

$$G_m = \left[\frac{y \cdot \rho_G \cdot (\rho_L - \rho_G)}{C_f \cdot \mu_l^{0.1}}\right]^{0.5} \tag{10.25}$$

where μ_l is the dynamic viscosity of water/wastewater being treated by ammonia stripping (kg/(m·s) or Pa.s), and C_f is a unitless packing factor, which is a value available from packing suppliers or can be sourced for common packing types in reference texts such as Crittenden *et al.* (2005). Because the water/wastewater flow is incompressible (unlike the extractant gas flow), further calculations to determine column diameter prefers the use of L_m (instead of G_m) where L_m can be calculated as follows:

$$L_m = \left(\frac{Q_L}{Q_G}\right) \cdot \left(\frac{\rho_L}{\rho_G}\right) \cdot G_m \tag{10.26}$$

The diameter of the packed column is then calculated as follows:

$$D_t = \left(\frac{4 \cdot Q_L \cdot \rho_L}{\pi \cdot L_m}\right)^{0.5} \tag{10.27}$$

There is an important interplay between the nominally selected values of S and column gas pressure drop in the column diameter calculations, simultaneously influencing operational costs by increased gas delivery pressure to overcome in the imposed pressure drop, and influencing capital costs via increasing or decreasing column diameter. For this reason, the designer typically iterates the calculations above until a suitable compromise is reached between operational and capital costs of the design. However, column supplier design software packages incorporate these considerations and others to provide an optimized design for a particular application.

By mass balance analysis it can be shown that the required packing height (l, with units of m) can be calculated as follows (Crittenden *et al.*, 2005):

$$l = \frac{Q_L}{A \cdot K_L a} \cdot \left(\frac{S}{S-1}\right) \cdot \ln\left[\frac{1 + (C_{\text{in}}/C_{\text{out}}) \cdot (S-1)}{S}\right] \tag{10.28}$$

where C_{in} and C_{out} are the influent and effluent concentrations of the constituent undergoing mass transfer (in this case NH_3), A is the column cross-sectional area determined using the column diameter as calculated above.

A value of $K_L a$ can be estimated from Equation (10.14) once the values of $k_L a$ and $k_G a$ have been estimated using the Onda correlations, as follows (Crittenden *et al.*, 2005):

$$\begin{aligned}
k_L &= 0.0051 \cdot \left(\frac{L_m}{a_w \cdot \mu_l}\right)^{2/3} \cdot \left(\frac{\mu_l}{\rho_L \cdot D_L}\right)^{-0.5} \cdot (a_t \cdot d_p)^{0.4} \cdot \left(\frac{\rho_L}{\mu_L \cdot g}\right)^{-1/3} \\
k_G &= 5.23 \cdot (a_t \cdot D_G) \cdot \left(\frac{G_m}{a_t \cdot \mu_G}\right)^{0.7} \left(\frac{\mu_G}{\rho_G \cdot D_G}\right)^{1/3} \cdot (a_t \cdot d_p)^{-2} \\
a_w &= a_t \cdot \left[1 - \exp\left[-1.45 \cdot \left(\frac{\sigma_c}{\sigma}\right)^{0.75} \cdot \left(\frac{L_m}{a_t \cdot \mu_l}\right)^{0.1} \cdot \left(\frac{(L_m)^2 \cdot a_t}{(\rho_L)^2 \cdot g}\right)^{-0.05} \cdot \left(\frac{(L_m)^2}{\rho_L \cdot a_t \cdot \sigma}\right)^{0.2}\right]\right]
\end{aligned} \tag{10.29}$$

where g is acceleration due to gravity (9.81 m/s²), D_G is gas-phase diffusivity (m²/s), D_L is liquid-phase diffusivity (m²/s), σ is the liquid surface tension (kg/s²), σ_c is the critical surface tension of the selected packing (kg/s²), a_t is the specific surface area of the packing (/m), d_p is nominal packing diameter (m), μ_G is gas viscosity (kg/(m·s)), μ_L is water viscosity (kg/(m·s)), a_w is the wetted packing surface area (/m), $k_L a = k_L \cdot a_w$ and $k_G a = k_L \cdot a_w$, and L_m is the water mass loading rate (kg per m² per s). The values of a_t, d_p and σ_c correspond to the selected packing type and are sourced from a reference text for common packing types (e.g., Crittenden *et al.* (2005)) or from a packing supplier for specialist packing types.

In addition to the process design component as described above, packed columns include mechanical internals such as supports to hold the wetted weight of the packing, whilst allowing a free path for the gas and liquid (Sinnott, 1999). Liquid distributors are also important to provide an even distribution of liquid across packed columns, and restributors may also be used to collect liquid to the column walls to be redistributed over the packing medium (Sinnott, 1999). Lastly, hold-down plates or bed limiters can be used to prevent top layers of packing from being fluidized if short periods of high gas flow or surging occur or to limit the expansion of a bed of packing (Sinnott, 1999). Typically, the standard fittings developed by a packing manufacturer are to be specified (Sinnott, 1999). Columns are typically tall with packing heights ranging between 6.1 and 7.6 meters (United States Environmental Protection Agency, 2000). A consideration of the material of construction is also important when using sulfuric acid solution to recover ammonia in the form of ammonium sulfate, and this may require high-grade steel (e.g., AISI 316 stainless steel or Duplex steels 2304) or suitable structural plastic components tolerant of elevated operating temperatures.

10.4.3 Liquid-filled diffused gas-sparged systems

With a liquid-filled column/reactor, small bubbles are produced via diffused gas sparging to rise through the liquid column and cause liquid–gas mass transfer (Mead & Leibbert, 1998). An example of this application is a system by Anaergia (2016). Multiple columns/reactors operating in series may also help to emulate plug-flow behavior and thereby benefit from kinetic effects of the first-order rate of gas-liquid mass transfer (Equation (10.13)). Tanks in series could be physically separated, or potentially separated by internal baffles. The design would depend on the desired extent of ammonia recovery and the operating ammonia concentrations in the wastewater, pH, and temperature. To design a liquid-filled gas-sparged column/reactor, the liquid-phase constitutive balance is solved for an elected n number of complete-mixed reactors in series (Figure 10.23), as follows:

$$V\frac{\left[\mathrm{NH_3(aq)}\right]_n}{dt} = Q_L \cdot \left[\mathrm{NH_3(aq)}\right]_{in,n} - Q_L \cdot \left[\mathrm{NH_3(aq)}\right]_n - V \cdot K_L a \cdot \left(\left[\mathrm{NH_3(aq)}\right]_n - \frac{P_{\mathrm{NH3}}}{K_{H,\mathrm{NH3}}}\right) \tag{10.30}$$

where V is the liquid hold-up volume of each reactor, assumed to be constant, Q_L is the wastewater or liquid extractant flow-rate, also assumed to be constant (a dilute phase), $[NH_3(aq)]_n$ is the concentration of free ammonia inside the nth mixed reactor (also same as exit concentration), and $K_L a$, $K_{H,NH3}$ and P_{NH3} are as above, except for use of units consistent with the constitutive mass balance.

For the design, it is necessary to know the mass transfer coefficient $K_L a$. Correlations are available to estimate $K_L a$ in gas-sparged reactors (e.g., Treybal (1981)).

10.4.4 Ammonia stripping and absorption – case studies of implementation

10.4.4.1 Case study 1 – anaergia – ammonium recovery from anaerobically digested chicken manure

An example of this process is shown below in Figure 10.24 at an operating facility in a large chicken manure anaerobic digestion plant. Chicken manure, largely due to the high protein content, is high in ammonia and total N. When digested, the N is largely solubilized as ammonia in the liquid phase. Treatment of the liquid was achieved at the facility using a series of four CSTR tanks providing plug flow conditions. The ammonia strippers were supplied with waste heat from a 500 kW combined heat

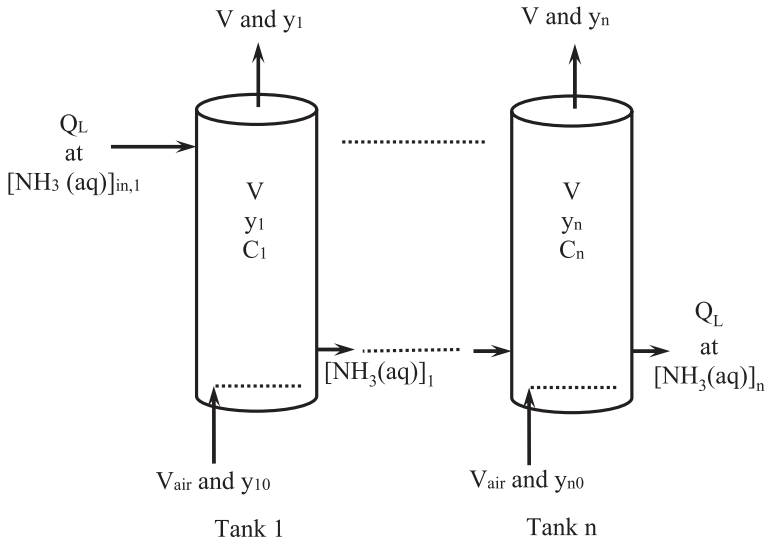

Figure 10.23 Schematic of liquid-filled columns/reactors in series to be used for gas–liquid mass transfer processes (i.e., stripping or absorption).

Figure 10.24 Operating ammonia recovery facility treating the digestate from a large poultry manure anaerobic digester (courtesy of Anaergia).

and power biogas generator. The concentrated ammonia gas was recovered using a single-stage vertical packed tower scrubber. The scrubber applied 93% sulfuric acid, thus transforming the ammonia gas into an acid salt fertilizer of ammonium sulfate.

10.4.4.2 Case study 2: nijhuis water technology B.V. – ammonia from anaerobic digestate

The N-load into an existing biological treatment plant was exceeding its capacity, with further increases forecast due to population growth in the catchment. The largest contributor to the plant, in terms of N-load, was digestate from a poultry slaughterhouse. An ammonia stripping process was installed to recover ammonia directly from the digestate and reduce the N-load into the biological process to defer the need to upgrade the biological process. The digestate flow was 75 m^3/d with a load of 2.5 g NH_4-N/L. The stripping process consisted of a heat exchanger, CO_2 stripper, ammonia stripper and a scrubber, and aimed to recover 70% of digestate ammonia. The influent was heated to 70°C, predominately through a tube-in-tube heat exchanger on the effluent flow, with additional heat input available from cogeneration plant offgas, that is to generate additional heating. Fresh air was injected into a CO_2 stripper tank to remove CO_2 and the high alkalinity in the digestate liquor ensured that the pH of the process stream could be increased to around 9.0 during CO_2 stripping without the addition of any chemicals, that is the loss of CO_2 raised pH.

Offgas from both CO_2 and ammonia strippers was treated in separate ammonia scrubbers with sulfuric acid added to produce ammonium sulgate. Recirculated air from the scrubber was used as carrier gas in the ammonia stripper and a polypropylene packing material (38 mm nominal size, 150 m^2/m^3 surface area) was added to the stripper to increase the effective contact surface area between liquid and gas phases (Figure 10.25). The stripper consistently achieved recovery efficiencies of 75–80% (even without caustic addition) and reduced the effluent ammonium concentration to 0.5–1.0

Figure 10.25 High surface area packing material used in the Nijhuis ammonia recovery system.

NH_4-N g/L. There was a decrease in pH and temperature throughout the stripping column, which reduced the recovery efficiency relative to the theoretical amount, however increasing the influent pH and temperature to allow for this reduction in pH and temperature could be implemented to increase recovery efficiency even further (albeit with an increase in operating costs).

In addition to costs associated with heating (0.4 €/kg N recovered), sulfuric acid (0.4 €/kg N), maintenance (0.10 €/kg N), and installed power (0.36 €/kg N), there was a cost associated with providing anti-scalant to prevent clogging in the stripper columns. Another solution could be to encourage scaling in the CO_2 stripping tank by reducing alkalinity and removing the precipitate mechanically, which increased capital costs slightly but reduced costs associated with scale removal by 0.35 €/kg N.

Costs associated with ammonium recovery from the digestate are offset slightly by the sale of recovered ammonium sulfate to local farmers, where the availability of local consumers for this scheme increased revenue from the sale of ammonium sulfate as well as contributing to creating a circular economy regarding waste treatment. At this site, ammonium sulfate was sold at a cost of 0.08 €/kg N. The cost effectiveness of the process increased at higher total ammoniacal N as a greater fraction of ammonia can be recovered at higher concentrations. At total ammoniacal N concentrations of >2 g/L, ammonium stripping was found to become more financially attractive than side-stream biological processes commonly applied to reduce the ammonium load in digestate returned to mainline biological treatment processes.

10.4.5 Ammonia stripping and absorption – challenges, opportunities, and research needs

As resources become more and more scarce and the demand for more sustainable agricultural practices increase, the need for N recovery will increase. While the technology can be economically applied using acid scrubbing agents like sulfuric acid, these too have sustainability concerns and inherent health and safety risks. Future research needs will focus on alternate scrubbing agents which can themselves be recovered from waste products (Jamaludin *et al.*, 2018). Moreover, as for struvite, regulatory and farmer's acceptance of the fertilizer product remains a challenge. Improved methods and technologies for recovering heat from, for example, onsite digesters or neighboring infrastructure, would reduce the energy demand for shifting equilibrium towards ammonia gas. This would lead to more installations in WWTPs. Scaling of packing material can lead to forced shutdown of stripping columns and reduced throughput. Thus, new methods for controlling scaling, in terms of understanding wastewater constituents that contribute to this in stripping columns and potentially removing them in targeted pre-treatments, would reduce the need for lengthy shutdowns. Additionally, there is still scope for developing new packing materials that promote better liquid–gas interactions, and further minimize fouling and scaling.

Better integration into wastewater treatment plant processes could consider ammonia stripping together with other resource recovery processes (e.g., struvite), could optimize whole-of-plant strategies for temperature and pH control, minimize chemical salts addition (e.g., caustic), and minimize the overall cost of N recovery.

10.5 SULFUR RECOVERY

Sulfur is one of the most abundant elements on earth and is essential for life, being a key constituent of many amino acids and an essential nutrient for plant growth. Until recently, elemental sulfur was mostly obtained by the Frasch hot-water method, by mining native sulfur associated with the caprock of salt domes, which often also held oil and natural gas (U.S. Geological Survey, 2002). Currently, due to the depletion of most sub-surface deposits, global sulfur production is mainly linked to petrochemical operations and recovered via the de Claus process (Eow, 2002).

Sulfur can prevail in many oxidation states and it exists in a great number of different chemical forms within its oxidation states (Cai *et al.*, 2017). Most of them play a very important role in aqueous

systems, where redox reactions occur either microbially or chemically following the thermodynamics of the system. Sulfur is highly redox sensitive and the many possible oxidation/reduction reactions make the sulfur chemistry quite complex. Sulfur species are also constituents of a large number of industrial products; for instance, sulfuric acid and sulfite and SO_2, and sulfides represent the major environmental pollutants. Additionally, hydrogen sulfide (H_2S), which is mainly found in gas form, is a significant human health hazard that causes death through asphyxiation.

This sub-section focuses on the basic principles and application of technologies for the recovery of sulfur from wastewater and biogas, which allow not only the recovery of an important resource that may become scarce when phasing out fossil resources, but also addresses possible environmental, health and economic issues derived from the presence of sulfur in those streams.

10.5.1 Conceptual overview

Sulfur can be present in the environment in many chemical forms. In what concerns sulfur recovery in the wastewater context, the focus lays mostly on hydrogen sulfide (H_2S), its most reduced form, either when: i) dissolved at high concentrations in industrial sour water, for example coming from the petrochemical sector; or ii) present in biogas produced by anaerobic digestion from organic-rich wastewater or waste activated sludge. Desulfurization technologies are, thus, key to treat those biogas/water streams so that they can be (re)used/valorized, also providing an opportunity for the recovery of sulfur. The most common approach to desulfurize biogas is to absorb H_2S in an alkaline solution in a counter-current scrubber similar to that described for ammonia removal in section 10.4. This sulfide-rich solution is regenerated in a biological oxidation step, in which sulfide is oxidized to elemental sulfur that can be recovered as a semi-solid or slurry.

10.5.2 Fundamental principles

The removal and recovery of sulfur from biogas requires two distinct steps, absorption of biogas in an aqueous solution and its biological oxidation. The removal of sulfides from liquid streams may only require the second of the two. In this sub-section, the key fundamental principles of both steps are briefly described.

10.5.2.1 Sulfide absorption

Sulfide in gaseous streams, for instance biogas, needs to be transferred into the liquid phase for treatment. Certain technologies can also treat sulfide in the gas phase, but they are either not applicable to the wastewater context or do not allow the recovery of sulfur (e.g., Clauss process, Sulfatreat process, etc).

Sulfide in aqueous solution is a weak acid and dissociates as follows:

$$H_2S_{aq} \rightleftarrows HS^- + H^+ \quad pK_1 = 7\,(20°C) \tag{10.31}$$

$$HS^- \rightleftharpoons S^{2-} + H^+ \quad pK_2 = 17\,(20°C) \tag{10.32}$$

H_2S has a high water solubility, ranging between 3000 and 4000 mg/L at atmospheric pressure and normal temperature. The H_2S solubility in water decreases with increasing temperatures.

Sulfide can be easily transferred from the gas to the liquid phases in absorption columns similar to those described in section 10.4. Since their principles design and operation are very similar, they will not be further discussed here. For H_2S absorption, alkaline solutions (pH >9–10) are needed to ensure >99% of H_2S is transferred from the gas to the liquid phase, and absorbed in their ionic forms.

10.5.2.2 Sulfide oxidation

Sulfide can be oxidized either chemically or biologically. Due to their ability to convert H_2S into elemental sulfur, sulfide oxidizing bacteria are suitable to be used in biological desulfurization processes. Chemical sulfide oxidation can also concomitantly take place. Both processes are discussed here.

Biological sulfide oxidation. A wide variety of microorganisms are known for their capability to oxidize reduced H_2S under a broad range of environmental conditions, for example Thioalkalivibrio, Thiobacillus, Thiomonas, and so on. (Kelly *et al.*, 1997; Sorokin *et al.*, 2011). The oxidation of sulfide yields energy, which enables bacterial growth. Oxidation of H_2S by sulfur oxidizing bacteria can be divided into phototrophic and chemotrophic processes. Phototrophic bacteria catalyze the so called 'van Niel' reaction under anaerobic conditions (Barton & Fauque, 2009), while chemotrophic ('colorless') sulfide oxidizing bacteria obtain their energy from the aerobic (with oxygen) or anoxic (with nitrate) oxidation of reduced sulfur compounds, for example sulfide, sulfur and sulfite.

The following general reactions describe the major phototrophic 'van Niel' biological hydrogen sulfide oxidation reactions:

$$H_2S + CO_2 + \text{light} \rightarrow (CH_2O)_n + H_2O + S^0 \tag{10.33}$$

$$H_2S + 2CO_2 + 2H_2O + \text{light} \rightarrow 2(CH_2O)_n + H_2SO_4 \tag{10.34}$$

The main chemotrophic biological hydrogen sulphide oxidation reactions are given by:

$$2H_2S + O_2 \rightarrow 2S^0 + 2H_2O \tag{10.35}$$

$$H_2S + 2O_2 \rightarrow H_2SO_4 \tag{10.36}$$

$$5H_2S + 8NO_3^- + 4H_2O \rightarrow 5H_2SO_4 + 4N_2 + 8OH^- \tag{10.37}$$

Abiotic sulfur conversions. Abiotic oxidation of H_2S with oxygen is relatively slow compared to oxidation by chemolithotrophic sulfide oxidizing microorganisms. The main oxidation product of abiotic oxidation is $S_2O_3^{2-}$ (O'Brien & Birkner, 1977):

$$2H_2S + 2O_2 \rightarrow S_2O_3^{2-} + H_2O + 2H^+ \tag{10.38}$$

Transformations of sulfur compounds can also occur as the result of chemical conversions when pH, temperature and oxidation-reduction conditions are favorable. Examples can be found in the formation of polysulfides (Kleinjan *et al.*, 2006), which form when elemental sulfur and dissolved sulfide react. Other sulfur compounds which can be chemically formed are inorganic elemental sulfur and thiosulfate. Chemically formed elemental sulfur is poorly dispersable in water, which is distinctively different when compared to sulfur formed by biological oxidation of sulfide. The origin of this hydrophilicity of biologically produced sulfur can be explained by adsorbed organic polymers such as proteins at the surface of the produced sulfur particles (Kleinjan, 2005).

Inorganic polysulfur compounds, that is polysulfide (S_x^{2-}) and their methylated form (R_2S_x), play a role in both biological and geological sulfur cycles as many biochemical mechanisms depend on this form of sulfur. In the presence of both sulfur and sulfide, polysulfides are formed according to (Roman *et al.*, 2014):

$$HS^- + (x-1)/8S_8 \rightarrow S_x^{2-} + H^+ \tag{10.39}$$

The polysulfide ions can be present in aqueous solution as complex mixtures of S_x^{2-} with $x \geq 2$. The formation of various polysulfide species is rapidly established based upon a chemical equilibrium. For biologically produced sulfur, the equilibrium constant is in on the order of $pK_x = 9.10$ (21°C) and polysulfides have an average chain length in of approximately the order of 4–5. The pK_x value for 'inorganically' produced sulfur is significantly lower ($pK_x = 8.78$; 21°C) (Kleinjan, 2005).

10.5.3 Applications and design

The basic concept of the biological desulfurization process (Thiopaq®) and recovery of elemental sulfur was first developed for the removal of H_2S from biogas in the late 1980s (Buisman *et al.*, 1990).

Biogas often contains some H_2S due to microbiological reduction of sulfur compounds, especially sulfate, present in the feed to anaerobic reactors. H_2S needs to be removed before combustion of the biogas to prevent the corrosion of the engines and their accelerated depreciation.

In the Tiopaq® process, H_2S-containing gas is humidified during bed irrigation, and subsequently contacted with microorganisms attached to a fixed bed (Graaf, 2012). One of the benefits of the process, next to the desulfurization of the gas stream, is the recovery of biologically produced elemental sulfur particles. The first full-scale facility for biogas desulfurization was built in 1993 in Eerbeek, the Netherlands (Janssen *et al.*, 2009). Since then, more than 270 installations have been built worldwide (Klok *et al.*, 2018), especially for desulfurization of biogas and several types of gas in the oil and gas industry. The technology is suitable for high pressure (up to 80 bar) as well as low pressure (below atmospheric pressure) feed gases and with a wide range of inlet H_2S concentrations. The operational parameters are shown in Table 10.2.

Biogas is typically a mixture of methane, carbon dioxide (CO_2), H_2S and higher alkanes. The composition and pressure of each gas varies widely and depends mainly on the gas source. Since H_2S and CO_2 are 'acidic gases', the Thiopaq process requires an alkaline solution to remove these compounds from a gas stream. The haloalkaline conditions which are applied in the process are established by a sodium carbonate/bicarbonate buffer solution (0.3–1.5 M) with a pH of 8.0–9.5. High CO_2 partial pressures will affect the removal of H_2S from gas streams when scrubbing the gas with an alkaline solution, and therefore the process requires elevated carbonate concentrations.

The process for desulfurization of 'sour' gas streams under haloalkaline conditions consists of three process steps (Figure 10.26): (1) absorption of H_2S in the process solution, (2) sulfide oxidation to elemental sulfur (S_8) in an aerated bioreactor and (3) removal of the formed S_8 from the suspension. In the first step, sour gas is directed to the bottom section of an absorber column, where it is put into contact with a counter current of washing solution, thereby consuming buffer capacity (see Table 10.3). The desulfurized gas, that is H_2S levels of <4 ppmv, leaves the absorber at the top for further processing.

The washing solution, containing the dissolved (bi)sulfide (HS^-), is fed to the bioreactor. Here, a mixed culture of sulfide oxidizing bacteria, dominated by *Thioalkalivibrio* spp., oxidize sulfide to primarily elemental sulfur (S_8), consuming O_2 as the final electron acceptor (Table 10.3, reaction 3). The O_2 is supplied to the bioreactor via the injection of air. In Figure 10.27, a scanning electron microscope (SEM) picture shows sulfide oxidizing bacteria excreting sulfur particles.

In addition to S_8, a fraction of sulfide is biologically oxidized to sulfate (SO_4^{2-}) (see Table 10.3, reaction 4). Besides biological oxidation, various chemical reactions can occur. Thiosulfate ($S_2O_3^{2-}$) is the main chemically formed intermediate of the oxidation of sulfide and polysulfide (Table 10.3, reactions 5 and 7). The selectivity for product formation depends on reactor conditions such as substrate levels, temperature and pH. The formation of sulfate and thiosulfate is unwanted for several

Table 10.2 General operational parameters (de Rink *et al.*, 2020; Driessen *et al.*, 2011; Echt *et al.*, 2017).

Parameter	Operational Window	Unit
Feed gas pressure	0–80	bar
H_2S levels in feed gas	0.05–100	% mol
Temperature	20–40	°C
Alkalinity/buffer capacity	0.3–1.5	$mol \cdot L^{-1}$
Conductivity of process solution	20–90	$mS \cdot cm^{-1}$
pH of process solution	8.0–9.5	–

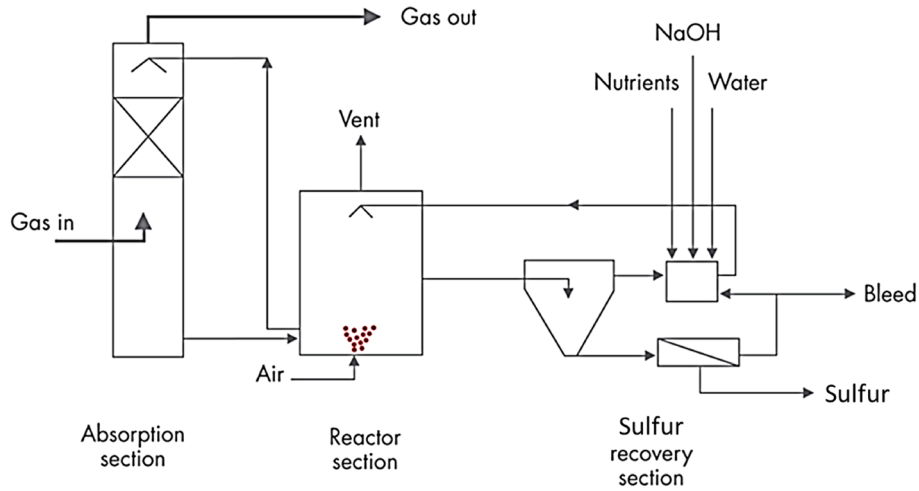

Figure 10.26 Flow scheme for the biological desulfurization process.

Table 10.3 Main reaction equations occurring in the biological desulfurization process. Bio: biological conversion. Chem: chemical conversion (from Klok (2015)).

	Reaction	Bio/Chem	Remarks
1	$H_2S_{(g)} \leftrightarrow H_2S_{(l)}$	Chem	–
2	$H_2S_{(l)} + OH^- \leftrightarrow HS^- + H_2O$	Chem	–
3	$HS^- + ½O_2 \rightarrow S^0 + OH^-$	Bio	–
4	$HS^- + 2O_2 \rightarrow SO_4^{2-} + H^+$	Bio	–
5	$2HS^- + 2O_2 \rightarrow S_2O_3^{2-} + H_2O$	Chem	–
6	$HS^- + (x–1)S^0 \leftrightarrow S_x^{2-} + H^+$	Chem	pH >8.0
7	$S_x^{2-} + 1½O_2 \rightarrow S_2O_3^{2-} + (x–2)S^0$	Chem	–

reasons. First, (thio)sulfate formation leads to the formation of protons and thus acidification of the medium, leading to more caustic consumption. Second, the addition of make-up water is required as (thio)sulfate can only be removed via a bleed stream, which is a waste stream purged from the process to control salinity levels. To optimize the formation of S_8, the bioreactor is operated at low oxygen/low oxidation-reduction potential (ORP) levels (i.e., ORP values below –200 mV) (Janssen *et al.*, 1998).

The effluent of the bioreactor i s primarily recirculated to the top of the absorber. In addition, a side flow from the reactor is directed to a gravity settler to remove sulfur from the process. From the bottom of the settler, a sulfur slurry is directed to a decanter centrifuge to further dewater the sulfur and form a sulfur cake. Nutrients to promote the growth of the bacteria, water and a concentrated caustic solution are added to the filtrate before the stream is returned to the bioreactor.

10.5.4 Case studies of implementation

The Thiopaq® process can be applied to the treatment of various H_2S-rich gaseous streams, including biogas, natural gas, and so on. An example of a full scale Thiopaq® installation can be found at

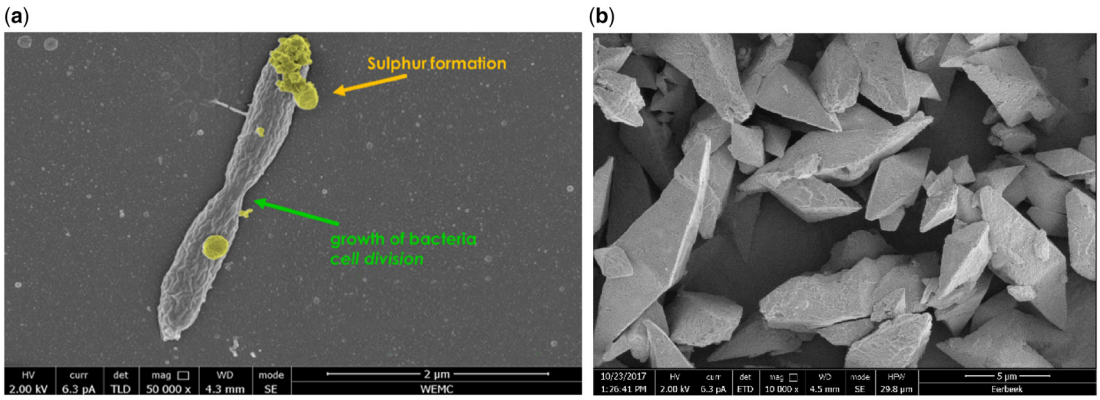

Figure 10.27 (a) Scanning electrode microscopy (SEM) picture of sulfide oxidizing bacteria excreting sulfur particles. Sulfur is artificially colored yellow for clarity. (b) Sulfur crystals in the final product.

an oil field in Southern Illinois, USA, containing over 200 smaller production wells. While not an example of desulfurization and sulfur recovery applied to the water sector, it is a very comprehensive example of S-recovery from an H_2S-rich gaseous stream and similar principles can be applied to the desulfurization of biogas.

The oil field considered here covers about 40 km^2 and produces approximately 1500 barrels of oil per day. Oil wells may contain natural gas, which is released during crude oil extraction. This so-called associated gas contains valuable condensable hydrocarbon liquids but is usually considered as waste in oil production. At the oil field in Southern Illinois, the associated gas had been flared for over 70 years, oxidizing H_2S in the feed gas and emitting substantial amounts of SO_2 to the atmosphere.

In order to reduce SO_2 emission levels for improvement of air quality, and to recover the condensable hydrocarbons, a Thiopaq and a liquefied petroleum gas (LPG; a mixture of propane and butane) recovery system were installed for gas treatment. The biological desulfurization plant (Thiopaq O&G) was commissioned in 2006 (see Figure 10.28(b)) (Lanning *et al.*, 2008). As the facility was 'skid built', all equipment was built to be road transportable, and consequently two smaller bioreactors instead of one large bioreactor were constructed (see Figure 10.28(a)).

The feed gas flow to the absorber is approximately between 800 and 1100 normal cubic meters·h^{-1} at a pressure of 4 bar. The major components in the gas are specified in Table 10.4 (Roman *et al.*, 2016). The feed gas contains concentrations of H_2S from 1 to 5 mol%, resulting in a total sulfide loading of 1–1.4 tons of sulfur per day (Figure 10.28(c)). The treated gas stream (i.e., <4 ppmv H_2S) is directed to an LPG recovery section where the LPG is recovered and stored. After LPG recovery, the remaining gas (~60 mol% CH_4 and ~30 mol% C_2H_6) is sold to the local distribution grid.

10.5.5 Challenges, opportunities and research needs

The activity and selectivity of the microorganisms are vital parameters in the design and operation of any biotechnological process. In the case of the biological desulfurization process, the fraction of sulfide which is converted into elemental sulfur should be maximized. In the current process, the selectivity of the sulfide to elemental sulfur conversion amounts to 90–94%. Hence, a significant amount of sulfuric acid is still formed, which requires the addition of caustic and results in formation of more bleed. When the selectivity towards sulfur formation is increased, the process becomes more efficient, resulting in lower caustic consumption and bleed formation. The latter is a side-stream, that is waste stream, of the process solution to control salinity levels. In full-scale facilities, two main factors determine the operational costs: (i) consumption of chemicals and (ii) formation of a

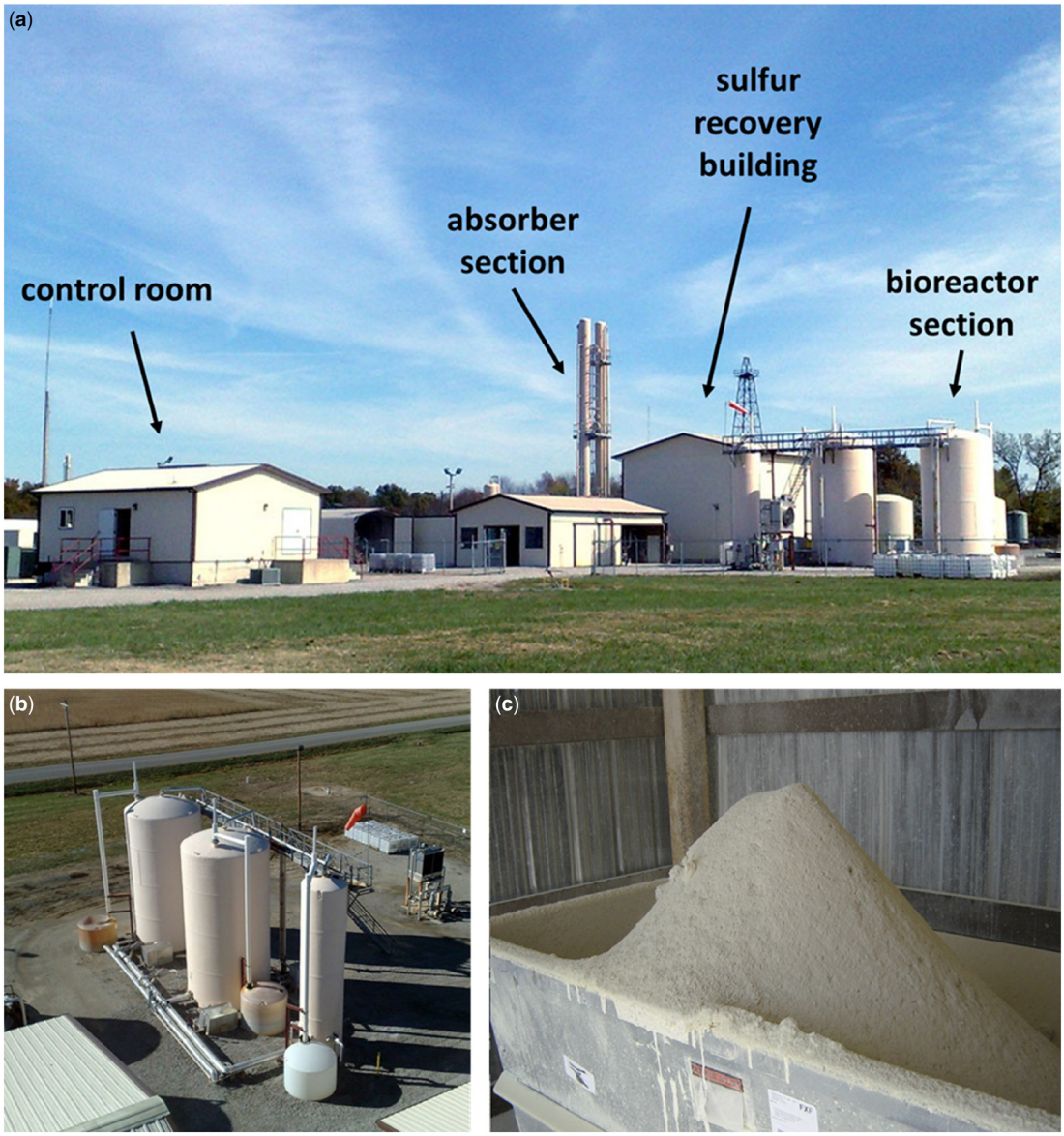

Figure 10.28 Pictures of the Thiopaq facility in Southern Illinois. (a) Overview picture of the facility with control room, absorber section, bioreactor section and sulfur recovery section. (b) Picture of the bioreactor section. (c) Picture of the recovered sulfur cake from the decanter centrifuge.

waste stream (bleed stream). Both factors are associated with the biological formation of sulfate and chemical formation of thiosulfate. Biological desulfurization plants yielding over 150 tons of sulfur per day would become economically feasible when selectivity for sulfur formation increases to >98%, which would largely reduce the largest operational costs. Improving selectivity towards elemental sulfur formation represents a challenge for future research.

Table 10.4 Inlet and outlet gas composition of the biological desulfurization unit found at an oil well in southern illinois (Roman *et al.*, 2016).

Component	Inlet Gas	Outlet Gas
H_2S	1–5 vol. %	<4 ppm(v)
CO_2	1–3 vol. %	<2 vol. %
CH_4	40–50 vol. %	40–50 vol. %
C_2H_6	15–20 vol. %	15–20 vol. %
C_3H_8	12–17 vol. %	12–17 vol. %
C_4+	10–15 vol. %	10–15 vol. %
H_2O	<2 vol. %	Saturated

10.6 CHAPTER SUMMARY

This chapter describes the fundamental principles of P, N and S recovery by three very different mixtures of physical, chemical and biological approaches; P-recovery by struvite precipitation invoking concepts of crystallization, N-recovery by stripping employing concepts of liquid–gas phase equilibrium, mass transfer and extraction, and S-recovery by an essentially biological process. While the theory underpinning each of the technologies is very different, they all provide a way to stem the loss of critical nutrients to the environment. Furthermore, they are faced by similar challenges with regards to product (i.e., purity, legislation, finding suitable end users) and operation (how best to integrate into other processes, interference from other components in wastewaters etc). Nonetheless, all technologies are being applied at full scale and have shown the potential to be economically feasible. Their economically feasibility will only increase as each nutrient becomes more limited and their value increases. Improvements in recovering energy (e.g., better heat exchanges, renewable sources etc), will further increase the uptake of ammonia recovery by stripping. Similar developments in the other technologies, coupled with increasing demand, will increase the number of their installations. This will in turn lead to greater awareness and acceptance of the final products, and ultimately the establishment of markets for these nutrients recovered from wastewaters.

10.7 EXERCISES

A landfill site produces leachate at a liquid flowrate of 5 m^3/h with a total ammoniacal nitrogen concentration of 700 mg NH_4-N/L at pH 9.5 and 80°C ($\rho_l = 971.76\ kg/m^3$; $\mu_L = 3.537 \times 10^{-4}$ Pa.s; $\sigma = 0.0626$ N/m). A stripping column is to be designed using a random packed tower containing Plastic tellerettes packing ($C_f = 20$; $a_t = 112\ m^2/m^3$; $d_p = 0.0508$ m; $\sigma_c = 0.033$ N/m; (Crittenden *et al.*, 2005)) to remove 95% of the free ammonia from the leachate using air at 80°C and 1 atm as the extractant gas ($\rho_G = 1\ kg/m^3$; $\mu_G = 20.88 \times 10^{-6}$ Pa.s). This aims to assist the final polishing of any remaining ammonia from the leachate in a subsequent biological nutrient removal plant.

Phase equilibrium for the dissolution of gaseous NH_3 in water can be described by Henry's Law, $K_{H,NH_3} = 1818$ Pa/M at 298 K (Sander, 2015), with $\Delta H^0/R$ for the dissolution of ammonia from air into water being 4100 (Sander, 2015). Diffusivity of ammonia in air is $D_G = 0.28 \times 10^{-4}\ m^2/s$ (Incropera & DeWitt, 2001), and diffusivity of ammonia in water is $D_L = 2 \times 10^{-9}\ m^2/s$ (Perry & Green, 1997; Table 2-372).

Exercise 10.1: Determine Henry's Law constant under the operating conditions.

Exercise 10.2: What is the dimensionless Henry's Law constant?

Exercise 10.3: What is the minimum gas flowrate for stripping the ammonia?

Exercise 10.4: Determine the diameter of a stripping column appropriate for the application.

Exercise 10.5: Determine the height of the stripping column.

10.8 DISCUSSION QUESTIONS

Question 10.1: What are the advantages and disadvantages of struvite precipitation on a sidestream (sludge) line treating digestate from an anaerobic digester. Can struvite precipitation be applied to the water mainline at a WWTP?

Question 10.2: What are the pollutants of concern if struvite is recovered from a municipal wastewater treatment plant and is to be used as a fertilizer in agriculture? To answer this, refer to relevant legislation.

Question 10.3: Nutrient recovery in WWTPs is slowly being implemented worldwide, please comment on the sentence: 'the bottleneck is not the technology but finding a welcoming market and suitable regulations'.

Question 10.4: How feasible would it be to implement P recovery in the following scenarios? For this, reflect on a likely amount and concentration of nutrients in the wastewater in each case, and think about a suitable technology (or technologies):

>100 000 PE WWTP with BNR and sludge stabilization through thermal processing
200 000 PE WWTP with BNR and sludge stabilization through Cambi (AD)
20 000 PE WWTP with BNR and sludge dewatering. Sludge is stabilized in nearby WWTP
10 000 PE WWTP with trickling filters + chemical P removal + and sludge dewatering. Sludge is stabilized in nearby WWTP
Decentralized system – one block of flats with yellow and black water separation

Question 10.5: Using the principles of a first-order reaction, explain why multiple tanks in series would be a more efficient process to air strip ammonia from a liquid slurry which contains 5000 mg/L NH_3-N?

Question 10.6: Select three different temperatures and pH levels which achieve an ammonia unionization of at least 90% NH_3. Discuss the implications of how to achieve the conditions from a chemical and thermodynamic perspective.

Question 10.7: Discuss consequences of choosing a higher/lower temperature for ammonia stripping in terms of effect of mass transfer coefficient and ammonia/ammonium equilibrium?

Question 10.8: Describe how fouling may affect efficacy of ammonia recovery (in terms of mass transfer, flooding, packing parameters etc)?

Question 10.9: Can stripping and struvite precipitation be implemented in the same process? Discuss.

ACKNOWLEDGEMENTS

Marcel Giesbers of the Wageningen Electron Microscopy Centre (WEMC) kindly provided the SEM pictures in Figure 10.27.

REFERENCES

Anaergia (2016). Ammonia stripper. United states patent US 2016/0130158 A1. Available at: http://www.patentsencyclopedia.com/imgfull/20160130158_01 (accessed 21 April 2021).

Anaergia (2020). Your Partner for a More Sustainable World. Turning Waste into Renewable Energy, Fertilizer, and Water for Reuse. Available at: https://www.swx.global/wp-content/uploads/2020/09/Anaergia-Product-Line.pdf (accessed 21 April 2021).

Anne C. O., Trebouet D., Jaounen P. and Quemeneur F. (2001). Nanofiltration of seawater: fractionation of mono- and multi-valent cations. *Desalination*, **140**, 67–77.

Barton L. L. and Fauque G. D. (2009). Biochemistry, physiology and biotechnology of sulfate-reducing bacteria. In: Advances in Applied Microbiology, A. J. Laskin, S. Sariaslani and G. M. Gadd (eds.), Academic Press, Amsterdam, The Netherlands, Vol. **68**, pp. 41–98.

Brockmann M. (2015). Struvia Technology for Phosphorus Recovery. Re-Water Braunschweig, 2–3 November 2015, Braunschweig, Germany.

Buisman C. J. N., Geraats B. G., Ijspeert P. and Lettinga G. (1990). Optimization of sulphur production in a biotechnological sulphide-removing reactor. *Biotechnology and Bioengineering*, **35**(1), 50–56.

Cai J., Zheng P., Quaisar M. and Zhang J. (2017). Elemental sulfur recovery of biological sulfide removal process from wastewater: a review. *Critical Reviews in Environmental Science and Technology*, **47**(21), 2079–2099.

Chen Y., Feng Y., Deveaux J. G., Masoud M. A., Chandra F. S., Chen H., Zhang D. and Feng L. (2019). Biomineralization forming process and bio-inspired nanomaterials for biomedical application: a review. *Minerals*, **9**(2), 1–21.

Chimenos J. M., Fernandez A. I., Hernandez A., Haurie L., Espiell F. and Ayora C. (2006). Optimization of phosphate removal in anodizing aluminum wastewater. *Water Research*, **40**(1), 137–143. https://doi.org/10.1016/j.watres.2005.10.033

Cordell D. and White S. (2015). Tracking phosphorus security: indicators of phosphorus vulnerability in the global food system. *Food Security*, **7**(2), 337–350.

Crittenden J. C., Trussell R. R., Hand D. W., Howe K. J. and Tchobanoglous G. (2005). Water Treatment Principles and Design, 2nd edn. John Wiley & Sons, Hoboken, New Jersey.

De Ridder M., de Jong S., Polchar J. and Lingemann S. (2012). Risks and Opportunities in the Global Phosphate Rock Market. Available at: www.hcss.nl (accessed 9 October 2019).

de Rink R., Klok J. B. M., van Heeringen G. J., Keesman K. J., Janssen A. J. H., ter Heijne A. and Buisman C. J. N. (2020). Biologically enhanced hydrogen sulfide absorption from sour gas under haloalkaline conditions. *Journal of Hazardous Materials*, **383**, 1–8.

Doyle, J. D. and Parsons, S. A. (2002). Struvite Formation, Control and Recovery. *Water Research*, **36**, 3925–3940.

Driessen W., Zessen E. and Visser M. (2011). Full-Scale Expererience with Biological Biogas Desulphurization Using the Thiopaq Technology. 16th European Biosolids and Organic Resources Conference, Leeds, UK.

Echt B., Leppin D., Mamrosh D., Mirdadian D., Seeger D. and Warren B. (2017). Low-Tonnage Sulfur Removal and Recovery. Laurance Reid Gas Conditioning Conference, Norman, Oklahoma.

Eckert J. S. (1961). Design techniques for sizing packed towers. *Chemical Engineering Progress*, **57**(9), 54–58.

Egle L., Rechberger H. and Zessner M. (2015). Overview and description of technologies for recovering phosphorus from municipal wastewater. *Resources, Conservation and Recycling*, **105**, 325–346.

Eow J. (2002). Recovery of sulfur from sour acid gas: a review of the technology. *Environmental Progress and Sustainable Energy*, **21**(3), 143–162.

Erisman J. W., Sutton M. A., Galloway J., Klimont Z. and Winiwarter W. (2008). How a century of ammonia synthesis changed the world. *Nature Geoscience*, **1**(10), 636–639.

Etter B., Tilley E., Khadka R. and Udert K. (2011). Low-cost struvite production using source-separated urine in Nepal. *Water Research*, **45**(2), 852–862.

European Sustainable Phosphorus Platform (2019). Success Stories. Available at: https://www.phosphorusplatform.eu/success-stories (accessed 4 October 2019).

FuturEnviro (2017). Spain's First Phosphorus Recovery Plant. June, 2017. Available at: https://futurenviro.es/en/spains-first-phosphorus-recovery-plant/ (accessed 12 December 2021).

Galbraith S. C., Schneider P. A. and Flood A. E. (2014). Model-driven experimental evaluation of struvite nucleation, growth and aggregation kinetics. *Water Research*, **56**, 122–132.

Galloway J. N., Winiwarter W., Leip A., Leach A. M., Bleeker A. and Erisman J. W. (2014). Nitrogen footprints: past, present and future. *Environmental Research Letters*, **9**(11), 1–11.

Graaf M. D. (2012). Biological Treatment of Spent Caustics Under Haloalkaline Conditions Using Soda Lake Bacteria. Wageningen University, the Netherlands.
Hinckley E.-L. S., Crawford J. T., Fakhraei H. and Driscoll C. T. (2020). A shift in sulfur-cycle manipulation from atmospheric emissions to agricultural additions. *Nature Geoscience*, **13**(9), 597–604.
Incropera F. and DeWitt D. (2001). Frank Incropera's Introduction to Heat Transfer, 4th edn. Wiley, Hoboken, New Jersey, USA.
Jamaludin Z., Rollings-Scattergood S., Lutes K. and Vaneeckhaute C. (2018). Evaluation of sustainable scrubbing agents for ammonia recovery from anaerobic digestate. *Bioresource Technology*, **270**, 596–602.
Janssen A. J. H., Meijer S., Bontsema J. and Lettinga G. (1998). Application of the redox potential for controling a sulfide oxidizing bioreactor. *Biotechnology and Bioengineering*, **60**(2), 147–155.
Janssen A. J. H., Lens P. N. L., Stams A. J. M., Plugge C. M., Sorokin D. Y., Muyzer G., Dijkman H., Van Zessen E., Luimes P. and Buisman C. J. N. (2009). Application of bacteria involved in the biological sulfur cycle for paper mill effluent purification. *Science of the Total Environment*, **407**(4), 1333–1343.
Kataki S., West H., Clarke M. and Baruah D. C. (2016). Phosphorus recovery as struvite: Recent concerns for use of seed, alternative Mg source, nitrogen conservation and fertilizer potential. *Resources, Conservation and Recycling*, **107**, 142–156.
Kelly D. P., Shergill J. K., Lu W.-P. and Wood A. P. (1997). Oxidative metabolism of inorganic sulfur compounds by bacteria. *Antonie van Leeuwenhoek*, **71**(1), 95–107.
Kleinjan W. (2005). Biologically Produced Sulfur Particles and Polysulfide Ions: Effects on a Biotechnological Process for the Removal of Hydrogen Sulfide from Gas Streams. PhD thesis, Wageningen University, The Netherlands.
Kleinjan W. E., Lammers J. N. J. J., de Keizer A. and Janssen A. J. H. (2006). Effect of biologically produced sulfur on gas absorption in a biotechnological hydrogen sulfide removal process. *Biotechnology and Bioengineering*, **94**(4), 633–644.
Klok J. B. M. (2015). Modeling Studies of Biological Gas Desulfurization under Haloalkaline Conditions. PhD thesis, Wageningen University, The Netherlands.
Klok J. B. M., Heeringen G. V., Rink R. D., Wijnbelt H. and Bowerbank G. (2018). Techno-Economic Impact of the Next Generation Thiopaq O&G Process for Sulfur Removal. 26th Annual Technical Conference, GPA-GCC & GPA Europe.
Leng Y. and Soares A. (2018). Understanding the Fundamentals of Bio-struvite Biomineralization in Wastewater. Cranfield University, Swindon, UK.
Lanning A., O'Brien M. and Mirdadion D. (2008). Straded no More – Turning Sour Casinghead Gas into Profits Using Shell-Paques Bio-Desulfurization. Laurance Reid Gas Conditioning Conference, Norman, Oklahoma.
Le Corre K. S. (2006). Understanding Struvite Crystallisation and Recovery. Cranfield University, Swindon, UK.
Le Corre K. S., Valsami-Jones E., Hobbs P. and Parsons S. A. (2009). Phosphorus recovery from wastewater by struvite crystallization: a review. *Critical Reviews in Environmental Science and Technology*, **39**(6), 433–477.
Lee A., Weon S., Lee C. and Koopman B. (2003). Removal of nitrogen and phosphate from wastewater by addition of bittern. *Chemosphere*, **51**, 265–271.
Li B., Boiarkina I., Yu W., Huang H. M., Munir T., Wang G. Q. and Young B. R. (2019a). Phosphorous recovery through struvite crystallization: challenges for future design. *Science of the Total Environment*, **648**, 1244–1256.
Li H., Yao Q., Dong Z., Zhao T., Zhou G. and Fu S. (2019b). Controlled synthesis of struvite nanowires in synthetic wastewater. *ACS Sustainable Chemistry and Engineering*, **7**(2), 2035–2043.
Ma H., Guo Y., Quin Y. and Li Y. (2018). Nutrient recovery technologies integrated with energy recovery by waste biomass anaerobic digestion. *Bioresource Technology*, **269**, 520–531. https://doi.org/10.1016/j.biortech.2018.08.114
Matassa S., Batstone D. J., Hulsen T., Schnoor J. and Verstraete W. (2015). Can direct conversion of used nitrogen to new feed and protein help feed the world? *Environmental Science & Technology*, **49**(9), 5247–5254.
Matsumiya Y., Yamasita T. and Nawamura Y. (2000). Phosphorus removal from sidestreams by crystallisation of magnesium-ammonium-phosphate using seawater. *Journal of the Chartered Institution of Water and Environmental Management*, **14**, 291–296.
Mbamba C. K., Tait S., Flores-Alsina F. and Batstone D. J. (2015). A systematic study of multiple minerals precipitation modelling in wastewater treatment plants, *Water Research*, **85**, 359–370.
McCarty P. L. (2018). What is the best biological process for nitrogen removal: when and why? *Environmental Science & Technology*, **52**(7), 3835–3841.

Mead E. and Leibbert J. (1998). A Comparison of Packed-Column and Low-Profile Sieve Tray Air Strippers. Conference on Hazardous Waste Research, May 18–21, Snowbird, Utah.
Mehta C. M. and Batstone D. J. (2013). Nucleation and growth kinetics of struvite crystallization. *Water Research*, **47**(8), 2890–2900.
Mehta C. M., Khunjar W. O., Nguyen V., Tait S. and Batstone D. J. (2015). Technologies to recover nutrients from waste streams: a critical review. *Critical Reviews in Environmental Science and Technology*, **45**(4), 385–427.
Mersmann A. (2001). Crystallization Technology Handbook. Marcel Dekker Inc., New York.
Muhmood A., Lu J., Dong R. and Wu S. (2019). Formation of struvite from agricultural wastewaters and its reuse on farmlands: Status and hindrances to closing the nutrient loop. *Journal of Environmental Management*, **230**, 1–13. https://doi.org/10.1016/j.jenvman.2018.09.030
Munch, E. and Barr K. (2001). Controlled struvite crystallization for removing phosphorus from anaerobic digester sidestreams. *Water Research*, **35**, 151–159.
Muys M., Phukan R., Brader G., Samad A., Moretti M., Haiden B., Pluchon S., Roest K., Vlaeminck S. E. and Spiller M. (2021). A systematic comparison of commercially produced struvite: quantities, qualities and soil-maize phosphorus availability. *Science of the Total Environment*, **756**, 1–12.
O'Brien D. J. and Birkner F. B. (1977). Kinetics of oxygenation of reduced sulfur species in aqueous solution. *Environmental Science & Technology*, **11**(12), 1114–1120.
Oehmen A., Lemos P. C., Carvalho G., Yuan Z., Keller J., Blackall L. L. and Reis M. A. M. (2007). Advances in enhanced biological phosphorus removal: from micro to macro scale. *Water Research*, **41**(11), 2271–2300.
Ohlinger K. N., Young T. M. and Schroeder E. D. (1998). Predicting struvite formation in digestion. *Water Research*, **32**(12), 3607–3614.
Paltrinieri L., Remmen K., Muller B., Chu L., Koser J., Wintgens T., Wessling M., de Smet L. and Sudholter E. (2019). Improved phosphoric acid recovery from sewage sludge ash using layer-by-layer modified membranes. *Journal of Membrane Science*. **587**, 1–9.
Perry R. and Green D. (1997). Chemical Engineers Handbook, 7th edn. McGraw-Hill, New York, USA.
Pikaar I., Sharma K. R., Hu S., Gernjak W., Keller J. and Yuan Z. (2014). Reducing sewer corrosion through integrated urban water management. *Science*, **345**(6198), 812–814.
Pratt C., Parsons S., Soares A. and Martin B. (2012). Biologically and chemically mediated adsorption and precipitation of phosphorus from wastewater. *Current Opinion in Biotechnology*, **23**(6), 890–896.
AirPrex (2015). Biosolids Treatment Optimization Process with the option of Phosphate Recoverye. MWEA Annual Biosolids Conference, Available from: https://www.mi-wea.org/docs/Forstner%20%20Biosolids%20Treatment%20Optimization%20Process.pdf (accessed: January 25 2022).
RecoPhos (2012). RecoPhos - Recovery of Phosphorus. Available from: http://www.recophos.org/ (accessed 25 January 2022).
Regy S., Mangin D., Klein J. P., Lieto J. (2001). Phosphate recovery by struvite precipitation in a stirred reactor. Centre Europeen d'Etudes des Polyphosphates. Available from: https://phosphorusplatform.eu/images/download/Regy-Mangin-Lagep-Report-struvite-precipitation-2001.pdf (accessed 25 January 2022).
Reijnders L. (2014). Phosphorus resources, their depletion and conservation, a review. *Resources, Conservation and Recycling*, **93**, 32–49.
Rittmann B. E., Mayer B., Westerhoff P. and Edwards M. (2011). Capturing the lost phosphorus. *Chemosphere*, **84**, 846–853.
Robles Á., Aguado D., Barat R., Borrás L., Bouzas A., Giménez J. B., Martí N., Ribes J., Ruano M. V., Serralta J., Ferrer J. and Seco A. (2020). New frontiers from removal to recycling of nitrogen and phosphorus from wastewater in the circular economy. *Bioresource Technology*, **300**, 1–18.
Robles-Aguilar A. A., Schrey S. D., Postma J. A., Temperton V. M. and Jablonowski N. D. (2020). Phosphorus uptake from struvite is modulated by the nitrogen form applied.. *Journal of Plant Nutrition and Soil Science*, **18**(1), 80–90.
Roman P., Bijmans M. and Janssen A. (2014). Quantification of individual polysulfides in lab-scale and full-scale desulfurisation bioreactors. *Environmental Chemistry*, **11**, 702–708.
Roman P., Klok J. B. M., Sousa J. A. B., Broman E., Dopson M., Van Zessen E., Bijmans M. F. M., Sorokin D. Y. and Janssen A. J. H. (2016). Selection and application of sulfide oxidizing microorganisms able to withstand thiols in gas biodesulfurization systems. *Environmental Science & Technology*, **50**(23), 12808–12815.
Romero-Güiza M. S., Astals S., Mata-Alvarez J. and Chimenos J. M. (2015). Feasibility of coupling anaerobic digestion and struvite precipitation in the same reactor: evaluation of different magnesium sources. *Journal of Chemical Engineering*, **270**, 542–548.

Sander R. (2015). Compilation of henry's law constants (version 4.0) for water as solvent. *Atmospheric Chemistry and Physics*, **15**, 4399–4981. https://doi.org/10.5194/acp-15-4399-2015 (accessed 25 January 2022).

Sekula-Wood E., Schnetzer A., Benitez-Nelson C., Anderson C., Berelson W., Brzezinski M., Burns J., Caron D., Cetinic I., Ferry J., Fitzpatrick E., Jones B., Miller P., Morton S., Schaffner R., Siegel D. and Thunell R. (2009). Rapid downward transport of the neurotoxin domoic acid in coastal waters. *Nature Geoscience*, **2**(4), 272–275.

Sena M. and Hicks A. (2018). Life cycle assessment review of struvite precipitation in wastewater treatment. *Resources, Conservation and Recycling*, **139**, 194–204.

Shaddel S., Ucar S., Andreassens J. P. and Osterhus S. W. (2019). Engineering of struvite crystals by regulating supersaturation – correlation with phosphorus recovery, crystal morphology and process efficiency. *Journal of Environmental Chemical Engineering*, **7**(1), 1–9.

Simoes F., Vale P., Stephenson T. and Soares A. (2018). The role of pH on the biological struvite production in digested sludge dewatering liquors. *Scientific Reports*, **8**, 1–9.

Sinnott R. K. (1999). Coulson and Richardson's Chemical Engineering, 3rd edn. Chemical Engineering Design, Butterworth-Heinemann, Jordan Hill, Oxford, Woburn, MA, vol. **6**.

Soares A, Veesam M., Simoes F., Wood E., Parsons S. A. and Stephenson T. (2014). Bio-Struvite: A new route to recover phosphorus from waste water. *CLEAN – Soil Air Water*, **42**(7), 994–997.

Sorokin D., Kuenen J. G. and Muyzer G. (2011). The microbial sulfur cycle at extremely haloalkaline conditions of soda lakes. *Frontiers in Microbiology*, **2**(44), 1–16.

Springer N. P. (2017). Physical, technical, and economic accessibility of resources and reserves need to be distinguished by grade: application to the case of phosphorus. *Science of the Total Environment*, **577**, 319–328.

Tait S., Solon K., Volcke E. I. P. and Batstone D. J. (2012). A Unified Approach to Modelling Wastewater Chemistry: Model Corrections. In: 3rd IWA/WEF Wastewater Treatment Modelling Seminar, 26–28 February, Mont-Sainte-Anne, Quebec, Canada.

Treybal R. E. (1981). Mass-transfer Operations, 3rd edn. McGraw-Hill Chemical Engineering Series. McGraw-Hill, Singapore.

Ueno, Y. and Fuji, M. (2001). Three years experience of operating and selling recov-ered struvite from full scale plant. *Environmental Technology*, **22**, 1373–1381.

United States Environmental Protection Agency (2000). Wastewater Technology Fact Sheet. Ammonia Stripping. EPA 832-F-00-019. September 2000. Available at: https://www3.epa.gov/npdes/pubs/ammonia_stripping.pdf (accessed 21 April 2021).

University of Florida (2015). Fluidization: A Unit Operation in Chemical Engineering, pp. 1–13. Available at: https://dl.icdst.org/pdfs/files1/be196045443d68512c1e012880d22888.pdf (accessed 16 December 2021).

U.S. Geological Survey (2002). Materials Flow of Sulfur. Available at: https://pubs.usgs.gov/of/2002/of02-298/of02-298.pdf (accessed 25 January 2022).

U.S. Geological Survey (2019). Mineral Commodity Summaries 2019. Available at: https://prd-wret.s3-us-west-2.amazonaws.com/assets/palladium/production/atoms/files/mcs2019_all.pdf (accessed 25 January 2022).

Vaneeckhaute C., Lebuf V., Michels E., Belia E., Vanrolleghem P. A., Tack F. M. G. and Meers E. (2017). Nutrient recovery from digestate: systematic technology review and product classification. *Waste and Biomass Valorization*, **8**(1), 21–40.

Wei J., Ge J., Rouff A., Wen X., Meng X. and Song Y. (2019). Phosphorus recovery from wastewater using light calcined magnesite, effects of alkalinity and organic acids. *Journal of Environmental Chemical Engineering*, **7**(5), 1–8.

Wu Y., Luo J., Zhang Q., Aleem M., Fang F., Xue Z. and Cao J. (2019). Potentials and challenges of phosphorus recovery as vivianite from wastewater: a review. *Chemosphere*, **226**, 246–258.

Yan Y., Xi X. R., Miao M., He T., Dong Z. H., Zhan K., Yan J. H., Zhao B. and Xia B. Y. (2018). Bio-inspired design of hierarchical FeP nanostructure arrays for the hydrogen evolution reaction. *Nano Research*, **11**(7), 3537–3547.